

Schrödingerization based Quantum Circuits for Maxwell's Equation with time-dependent source terms

Chuwen Ma ^{*} ^{†1,2}, Shi Jin ^{‡1,2,3}, Nana Liu ^{§2,3,4}, Kezhen Wang ^{¶1,2}, and Lei Zhang ^{||1,2,3}

¹School of Mathematical Sciences, Shanghai Jiao Tong University, Shanghai 200240, China.

²Institute of Natural Sciences, Shanghai Jiao Tong University, Shanghai 200240, China.

³Ministry of Education, Key Laboratory in Scientific and Engineering Computing,
Shanghai Jiao Tong University, Shanghai 200240, China.

⁴University of Michigan-Shanghai Jiao Tong University Joint Institute, Shanghai 200240,
China.

November 19, 2024

Abstract

The Schrödingerisation method combined with the autonomization technique in [10] converts general non-autonomous linear differential equations with non-unitary dynamics into systems of autonomous Schrödinger-type equations, via the so-called warped phase transformation that maps the equation into two higher dimension. Despite the success of Schrödingerisation techniques, they typically require the black box of the sparse Hamiltonian simulation, suitable for continuous-variable based analog quantum simulation. For qubit-based general quantum computing one needs to design the quantum circuits for practical implementation.

This paper explicitly constructs a quantum circuit for Maxwell's equations with perfect electric conductor (PEC) boundary conditions and time-dependent source terms, based on Schrödingerization and autonomization, with corresponding computational complexity analysis. Through initial value smoothing and high-order approximation to the delta function, the increase in qubits from the extra dimensions only requires minor rise in computational complexity, almost $\log \log 1/\varepsilon$ where ε is the desired precision. Our analysis demonstrates that quantum algorithms constructed using Schrödingerisation exhibit polynomial acceleration in computational complexity compared to the classical Finite Difference Time Domain (FDTD) format.

*Corresponding author.

[†]chuwenii@sjtu.edu.cn

[‡]shijin-m@sjtu.edu.cn

[§]nana.liu@quantumlah.org

[¶]carson-w@sjtu.edu.cn

^{||}lzhang2012@sjtu.edu.cn

1 Introduction

Maxwell's equations are fundamental for understanding electromagnetic phenomena across a broad spectrum of scales, from subatomic particles to galactic structures. The profound impact of electromagnetic field theory on both science and technology is evident, with applications that permeate nearly every aspect of modern life, particularly in fields such as electrical engineering, optics, wireless optical communication, and remote sensing. In the context of modern wireless communication, there is an exponential surge in demand for efficient signal processing capabilities. Traditional algorithms are increasingly inadequate to meet these growing requirements. Despite remarkable progress in addressing extensive physical systems through supercomputers [33, 51], obtaining solutions within a feasible computation time is still intractable.

Quantum technology has achieved significant progresses, notably demonstrating quantum advantage over classical computers [5, 14, 17, 32, 38, 39, 50]. Among many potential applications, one particularly promising area is the utilization of quantum computers to solve the time-dependent Schrödinger equations, which follow unitary evolutions and hence the wave functions can be coherently represented on quantum computers. A variety of efficient quantum algorithms have been developed in Hamiltonian simulations [2, 3, 7, 8, 11, 15, 28, 30, 31]. To this aim, it is convenient to rewrite the source-free Maxwell formulation into a Hamiltonian system based on the Riemann-Silberstein vectors for quantum simulation [9, 13, 40, 43–46].

When source terms or complex boundary conditions arise in electromagnetic field systems, the time evolution of the system often ceases to be unitary. Therefore, it is essential to transform these systems into unitary dynamical systems [1, 4, 10, 24, 25]. Among the unitarisation approaches, the Schrödingerisation method introduced in [24, 25] provides a simple and generic framework for quantum simulation of all linear partial differential equations (PDEs) and ordinary differential equations (ODEs). Its essence lies in employing a warped phase transformation that elevates the equations to one higher dimension. In the Fourier space, this transformation reveals a system of Schrödinger-type equations. The approach has been expanded to address a wide array of problems, including open quantum systems in bounded domains with non-unitary artificial boundary conditions [19], problems entailing physical boundary or interface conditions [18], Maxwell's equations [22], the Fokker-Planck equation [27], ill-posed scenarios such as the backward heat equation [23], linear dynamical systems with inhomogeneous terms [21], iterative linear algebra solvers [20], etc. Despite the significant success of Schrödingerisation, the explicit design of the corresponding quantum circuits for most problems remains to be addressed. Recently, quantum circuits based on Schrödingerisation have been designed for heat equations, advection equations [16] and heat equations with boundary conditions [26].

This paper details the explicit construction of quantum circuits derived from the quantum algorithms through the process of Schrödingerisation, in conjunction with the autonomization techniques in [10]. The main contributions of this paper are summarized as follows:

- We propose a quantum algorithm for Maxwell's equations under Perfect Electric Conductor (PEC) boundary conditions and time-varying source terms. This is accomplished by employing a stretching transformation to derive a homogeneous ordinary differential equation

(ODE) system [21], followed by the process of Schrödingerisation. Additionally, we apply the autonomization methodology in [10] to construct a time-independent (autonomous) Hamiltonian system in one higher dimension, characterized by a Hamiltonian operator with spatially varying coefficients.

- We construct the quantum circuits corresponding to the proposed quantum algorithms.
- We apply smooth extension and high-order approximations to the delta function, demonstrating that the increase in dimensionality resulting from Schrödingerisation and the technique of turning a time-dependent non-autonomous system to a time-independent autonomous only increases mildly the computational complexity on quantum computations, almost $\log \log 1/\varepsilon$ with ε the desired precision. We further show that transforming a source-driven ODE system into a homogeneous one by introducing auxiliary variables via a stretching transformation does not degrade the success probability of obtaining the target state (see Remark 5.1), thus maintaining the computational efficiency of the quantum algorithm.

The rest of the paper is organized as follows. In section 2, we present the matrix representation of Maxwell's equations with physical boundary conditions and time-varying source terms. In section 3, we give a brief review of the Schrödingerisation approach for general inhomogeneous linear ODEs induced from the discretization of Maxwell's equations, and turn the non-autonomous system into an autonomous one. In section 4, we present the detailed implementation of quantum circuits for the time-independent Hamiltonian system. In section 5, we show the computational cost of the explicit quantum circuit and demonstrate that the complexity of the quantum algorithm exhibits polynomial acceleration compared to classical algorithms. In section 6, we conduct numerical experiments to validate the feasibility of the proposed algorithm, specifically focusing on the accuracy of the recovery through Schrödingerisation and high-order convergence rates.

Throughout the paper, we restrict the simulation to a finite time interval $t \in [0, T]$, and we use a 0-based indexing, i.e. $j = \{0, 1, \dots, N-1\}$, or $j \in [N]$, and $|j\rangle \in \mathbb{C}^N$, to denote a vector with the j -th component being 1 and others 0. We shall denote the identity matrix and null matrix by I and $\mathbf{0}$, respectively, and the dimensions of these matrices should be clear from the context. Otherwise, The notation I_N stands for the N -dimensional identity matrix, and $\mathbf{1}$ denotes 2-dimension identity matrix.

2 The matrix representation of Maxwell's equations

In this section, we consider Maxwell's equations for a linear homogeneous medium with constant permittivity and permeability which are set to be 1, in the presence of sources of charge ρ and currents \mathbf{J} as

$$\frac{\partial}{\partial t} \mathbf{E} - \nabla \times \mathbf{B} = -\mathbf{J}, \quad \frac{\partial}{\partial t} \mathbf{B} + \nabla \times \mathbf{E} = \mathbf{0}, \quad (1a)$$

$$\nabla \cdot \mathbf{B} = 0, \quad \nabla \cdot \mathbf{E} = \rho, \quad (1b)$$

in the three dimensional domain $\Omega = [0, 1]^3$. From Equation (1), the Maxwell-Gauss equation (or Gauss's law) and the Maxwell-Thomson equation (1b) are actually consequences of the other equations and charge conservation equation

$$\frac{\partial \rho}{\partial t} = \nabla \cdot \mathbf{J}. \quad (2)$$

To simplify the notation, let

$$\begin{aligned} \mathcal{F} &= \left(E_x|0\rangle + E_y|1\rangle + E_z|2\rangle + r^a|3\rangle + B_x|4\rangle + B_y|5\rangle + B_z|6\rangle + r^b|7\rangle \right), \\ \mathcal{J} &= \left(J_x|0\rangle + J_y|1\rangle + J_z|2\rangle - \rho|7\rangle \right). \end{aligned}$$

Write Equation (1) in vector form as

$$\frac{\partial \mathcal{F}}{\partial t} = \mathcal{M}\mathcal{F} - \mathcal{J} = \begin{bmatrix} \mathbf{0} & \mathcal{M} \\ \mathcal{M}^\dagger & \mathbf{0} \end{bmatrix} \mathcal{F} - \mathcal{J}. \quad \mathcal{M} = \begin{bmatrix} 0 & -\partial_z & \partial_y & -\partial_x \\ \partial_z & 0 & -\partial_x & -\partial_y \\ -\partial_y & \partial_x & 0 & -\partial_z \\ \partial_x & \partial_y & \partial_z & 0 \end{bmatrix}. \quad (3)$$

By comparing (1) and (3), it is evident that the auxiliary variable $r^a \equiv r^b \equiv 0$. We consider the perfect electric conductor (PEC) boundary condition, which takes a specific form because a perfect conductor supports surface charges and currents, preventing fields from penetrating the body [6], i.e.,

$$\mathbf{n} \times \mathbf{E} = \mathbf{0}, \quad \mathbf{n} \cdot \mathbf{B} = 0, \quad \text{on } \partial\Omega, \quad (4)$$

where \mathbf{n} is the unit normal to the boundary $\partial\Omega$.

3 Schrödingerization for Maxwell's equations

In this section, we provide a brief review of the Schrödingerization [24, 25] of Maxwell's equations using Yee's scheme [22]. We choose a uniform spatial mesh size $\Delta x = \Delta y = \Delta z = M^{-1}$ with M an even positive integer given by $M = 2^m$.

3.1 Notations of finite difference operator

Before presenting the discretization, we introduce some notation. We define the shift operators as follows:

$$S^+|j\rangle = |j+1\rangle, \quad S^-|j\rangle = |j-1\rangle, \quad 1 \leq j \leq M-1.$$

It is straightforward to verify that the matrices can be expressed as

$$S^- = \sum_{j=1}^{2^m-1} |j-1\rangle\langle j| = \sum_{j=1}^m \mathbf{1}^{\otimes(m-j)} \otimes \sigma_{01} \otimes \sigma_{10}^{\otimes(j-1)} \triangleq \sum_{j=1}^m s_j^-, \quad (5)$$

$$S^+ = \sum_{j=1}^{2^m-1} |j\rangle\langle j-1| = \sum_{j=1}^m \mathbf{1}^{\otimes(m-j)} \otimes \sigma_{10} \otimes \sigma_{01}^{\otimes(j-1)} \triangleq \sum_{j=1}^m s_j^+, \quad (6)$$

$$I^r = \sum_{j=1}^{2^m-1} |j\rangle\langle j| = \mathbf{1}^{\otimes m} - \sigma_{00}^{\otimes m}. \quad (7)$$

Here $\sigma_{ij} := |i\rangle\langle j|$, $i, j = 0, 1$ is a 2×2 matrix. These two shift operators satisfy $S^+ = (S^-)^\dagger$. For a single qubit, the Pauli matrices are

$$X = \begin{bmatrix} 0 & 1 \\ 1 & 0 \end{bmatrix} = \sigma_{01} + \sigma_{10}, \quad Y = \begin{bmatrix} 0 & -i \\ i & 0 \end{bmatrix} = -i\sigma_{01} + i\sigma_{10}, \quad Z = \begin{bmatrix} 1 & 0 \\ 0 & -1 \end{bmatrix} = \sigma_{00} - \sigma_{11}.$$

3.2 Discretization of Maxwell's equations

According to Yee's lattice configuration [41, 49], the different components of the electromagnetic field and of the current densities are calculated at different cell center (half integer index) and cell vertices (integer index):

$$\begin{aligned} \mathbf{E}_j(t) &= (E_{x,j}, E_{y,j}, E_{z,j}) = (E_{x,j_1+\frac{1}{2},j_2,j_3}, E_{y,j_1,j_2+\frac{1}{2},j_3}, E_{z,j_1,j_2,j_3+\frac{1}{2}}), \\ \mathbf{B}_j(t) &= (B_{x,j}, B_{y,j}, B_{z,j}) = (B_{x,j_1,j_2+\frac{1}{2},j_3+\frac{1}{2}}, B_{y,j_1+\frac{1}{2},j_2,j_3+\frac{1}{2}}, B_{z,j_1+\frac{1}{2},j_2+\frac{1}{2},j_3}). \end{aligned}$$

Correspondingly, the current densities, charge densities and the auxiliary variables are located according to Yee's lattice configuration:

$$\begin{aligned} \mathbf{J}_j(t) &= (J_{x,j}, J_{y,j}, J_{z,j}) = (J_{x,j_1+\frac{1}{2},j_2,j_3}, J_{y,j_1,j_2+\frac{1}{2},j_3}, J_{z,j_1,j_2,j_3+\frac{1}{2}}), \\ \rho_j(t) &= \rho_{j_1,j_2,j_3}, \quad r_j^a = r_{j_1,j_2,j_3}^a, \quad r_j^b = r_{j_1+\frac{1}{2},j_2+\frac{1}{2},j_3+\frac{1}{2}}^b. \end{aligned}$$

Following Yee's algorithm, one gets the semi-discrete system:

$$\frac{d\mathbf{E}_h}{dt} - \nabla_h \times \mathbf{B}_h = -\mathbf{J}_h, \quad \frac{dr_h^a}{dt} = \nabla_h \cdot \mathbf{B}_h, \quad (8)$$

$$\frac{d\mathbf{B}_h}{dt} + \nabla_h \times \mathbf{E}_h = \mathbf{0}, \quad \frac{dr_h^b}{dt} = \nabla_h \cdot \mathbf{E}_h + \rho_h, \quad (9)$$

where \mathbf{E}_h , \mathbf{B}_h , \mathbf{J}_h , r_h^a and r_h^b are the collections of \mathbf{E}_j , \mathbf{B}_j , \mathbf{J}_j , r_j^a , and r_j^b for $0 \leq j_1, j_2, j_3 < M$,

$$\mathbf{E}_h = \begin{bmatrix} \sum_j E_{x,j} |\mathbf{j}\rangle \\ \sum_j E_{y,j} |\mathbf{j}\rangle \\ \sum_j E_{z,j} |\mathbf{j}\rangle \end{bmatrix}, \quad \mathbf{B}_h = \begin{bmatrix} \sum_j B_{x,j} |\mathbf{j}\rangle \\ \sum_j B_{y,j} |\mathbf{j}\rangle \\ \sum_j B_{z,j} |\mathbf{j}\rangle \end{bmatrix}, \quad \mathbf{J}_h = \begin{bmatrix} \sum_j J_{x,j} |\mathbf{j}\rangle \\ \sum_j J_{y,j} |\mathbf{j}\rangle \\ \sum_j J_{z,j} |\mathbf{j}\rangle \end{bmatrix}, \quad r_h^\alpha = \sum_j r_j^\alpha |\mathbf{j}\rangle, \quad \alpha = a, b. \quad (10)$$

The perfect electric conductor (PEC) boundary condition is given by

$$\begin{aligned} E_{x,j_1+\frac{1}{2},j_2,j_3} \Big|_{j_2=0 \text{ or } j_3=0} &\equiv 0, & E_{y,j_1,j_2+\frac{1}{2},j_3} \Big|_{j_1=0 \text{ or } j_3=0} &\equiv 0, & E_{z,j_1,j_2,j_3+\frac{1}{2}} \Big|_{j_1=0 \text{ or } j_2=0} &\equiv 0, \\ B_{x,j_1,j_2+\frac{1}{2},j_3+\frac{1}{2}} \Big|_{j_1=0} &\equiv 0, & B_{y,j_1+\frac{1}{2},j_2,j_3+\frac{1}{2}} \Big|_{j_2=0} &\equiv 0, & B_{z,j_1+\frac{1}{2},j_2+\frac{1}{2},j_3} \Big|_{j_3=0} &\equiv 0, \end{aligned}$$

for $0 \leq j_1, j_2, j_3 < M$ and $0 \leq t \leq T$. To satisfy the boundary condition, we set

$$J_{x,j_1+\frac{1}{2},j_2,j_3} \Big|_{j_2=0 \text{ or } j_3=0} \equiv 0, \quad J_{y,j_1,j_2+\frac{1}{2},j_3} \Big|_{j_1=0 \text{ or } j_3=0} \equiv 0, \quad J_{z,j_1,j_2,j_3+\frac{1}{2}} \Big|_{j_1=0 \text{ or } j_2=0} \equiv 0.$$

The discrete curl operator $\nabla_h \times$ is defined using central differences, which are also applied in the divergence operators. We define the difference matrices as follows

$$\mathbf{D}^- = \sum_{i=0}^{M-2} |i\rangle\langle i+1| - \sum_{i=1}^{M-1} |i\rangle\langle i| = S^- - \mathbf{I}^r, \quad (11)$$

$$\mathbf{D}^+ = \sum_{i=1}^{M-1} |i\rangle\langle i| - \sum_{i=1}^{M-1} |i\rangle\langle i-1| = \mathbf{I}^r - S^+. \quad (12)$$

It is evident that $D^- = -(D^+)^\dagger$. Using (11) and (12), we define the following matrices

$$D_x^+ = \frac{\mathbf{I}_M \otimes \mathbf{I}_M \otimes D^+}{\Delta x}, \quad D_y^+ = \frac{\mathbf{I}_M \otimes D^+ \otimes \mathbf{I}_M}{\Delta y}, \quad D_z^+ = \frac{D^+ \otimes \mathbf{I}_M \otimes \mathbf{I}_M}{\Delta z}, \quad (13)$$

$$D_x^- = \frac{\mathbf{I}_M \otimes \mathbf{I}_M \otimes D^-}{\Delta x}, \quad D_y^- = \frac{\mathbf{I}_M \otimes D^- \otimes \mathbf{I}_M}{\Delta y}, \quad D_z^- = \frac{D^- \otimes \mathbf{I}_M \otimes \mathbf{I}_M}{\Delta z}. \quad (14)$$

Next, we define the discrete curl operator

$$M_{\nabla_h \times}^E = \begin{bmatrix} \mathbf{0} & -D_z^+ & D_y^+ & -D_x^+ \\ D_z^+ & \mathbf{0} & -D_x^+ & -D_y^+ \\ -D_y^+ & D_x^+ & \mathbf{0} & -D_z^+ \\ D_x^+ & D_y^+ & D_z^+ & \mathbf{0} \end{bmatrix}, \quad M_{\nabla_h \times}^B = \begin{bmatrix} \mathbf{0} & D_z^- & -D_y^- & D_x^- \\ -D_z^- & \mathbf{0} & D_x^- & D_y^- \\ D_y^- & -D_x^- & \mathbf{0} & D_z^- \\ -D_x^- & -D_y^- & -D_z^- & \mathbf{0} \end{bmatrix}.$$

It follows that $M_{\nabla_h \times}^B = -(M_{\nabla_h \times}^E)^\dagger$. The matrix representation of (8)-(9) can be rewritten as an $n = 8M^3$ dimensional ODE system:

$$\frac{d}{dt} \mathbf{u} = A \mathbf{u} + \mathbf{f}, \quad A = \begin{bmatrix} \mathbf{0} & M_{\nabla_h \times}^E \\ M_{\nabla_h \times}^B & \mathbf{0} \end{bmatrix}, \quad (15)$$

where $\mathbf{u} = |0\rangle \otimes \mathbf{E}_h + |1\rangle \otimes r_h^a + |2\rangle \otimes \mathbf{B}_h + |3\rangle \otimes r_h^b$ and $\mathbf{f} = |0\rangle \otimes \mathbf{f}_1 + |1\rangle \otimes \mathbf{f}_2$ with $\mathbf{f}_1 = \begin{bmatrix} -\mathbf{J}_h \\ \mathbf{0} \end{bmatrix}$, $\mathbf{f}_2 = \sum_{j=0}^2 |j\rangle \otimes \mathbf{0} + |3\rangle \otimes \rho_h$, and $\mathbf{0} \in \mathbb{R}^{M^3}$ is a zero vector.

3.3 A review of general framework of Schrödingerisation

It is time to consider the Schrödingerization of the linear system with source terms introduced in [21],

$$\frac{d}{dt} \begin{bmatrix} \mathbf{u} \\ \mathbf{r} \end{bmatrix} = \begin{bmatrix} A & \mathbf{F} \\ \mathbf{0}^\top & \mathbf{0} \end{bmatrix} \begin{bmatrix} \mathbf{u} \\ \mathbf{r} \end{bmatrix} = \tilde{A} \begin{bmatrix} \mathbf{u} \\ \mathbf{r} \end{bmatrix}, \quad \begin{bmatrix} \mathbf{u}(0) \\ \mathbf{r}(0) \end{bmatrix} = \begin{bmatrix} \mathbf{u}_0 \\ \mathbf{r}_0 \end{bmatrix}, \quad (16)$$

where $\mathbf{r} = [c_0, c_0, \dots, c_0]^\top$, $c_0 = \max\{\max_{t \in [0, T]} \|\mathbf{f}\|_{l^\infty}, 1\}$ is a constant, and $\mathbf{F} = \sigma_{00} \otimes \mathbf{F}_1 + \sigma_{11} \otimes \mathbf{F}_2$ with $\mathbf{F}_1 = \text{diag}\{\mathbf{f}_1/c_0\}$ and $\mathbf{F}_2 = \text{diag}\{\mathbf{f}_2/c_0\}$. Since any matrix can be decomposed into a Hermitian matrix and an anti-Hermitian matrix, Equation (16) can be expressed as

$$\frac{d}{dt} \mathbf{u}_f = (H_1 + iH_2) \mathbf{u}_f, \quad H_1 = \frac{1}{2}(\tilde{A} + \tilde{A}^\dagger), \quad H_2 = \frac{1}{2i}(\tilde{A} - \tilde{A}^\dagger), \quad (17)$$

where $\mathbf{u}_f = |0\rangle \mathbf{u} + |1\rangle \mathbf{r}$ with H_1 and H_2 defined by

$$H_1 = \frac{1}{2} \begin{bmatrix} \mathbf{0} & \mathbf{0} & \mathbf{F}_1 & \mathbf{0} \\ \mathbf{0} & \mathbf{0} & \mathbf{0} & \mathbf{F}_2 \\ \mathbf{F}_1 & \mathbf{0} & \mathbf{0} & \mathbf{0} \\ \mathbf{0} & \mathbf{F}_2 & \mathbf{0} & \mathbf{0} \end{bmatrix}, \quad H_2 = \frac{1}{2i} \begin{bmatrix} \mathbf{0} & 2M_{\nabla_h \times}^E & \mathbf{F}_1 & \mathbf{0} \\ 2M_{\nabla_h \times}^B & \mathbf{0} & \mathbf{0} & \mathbf{F}_2 \\ -\mathbf{F}_1 & \mathbf{0} & \mathbf{0} & \mathbf{0} \\ \mathbf{0} & -\mathbf{F}_2 & \mathbf{0} & \mathbf{0} \end{bmatrix}, \quad (18)$$

both of which are Hermitian. Thus, the sparsity of H_1 equals to the sparsity of \tilde{A} . Using the warped phase transformation $\mathbf{w}(t, p) = e^{-p} \mathbf{u}_f$ for $p > 0$ and extending the initial data to $p < 0$, Equation (17) is converted to a system of linear convection equations [21]:

$$\begin{aligned} \frac{d}{dt} \mathbf{w} &= -H_1 \partial_p \mathbf{w} + iH_2 \mathbf{w}, \\ \mathbf{w}(0) &= g(p) \mathbf{u}_f(0), \end{aligned} \quad (19)$$

with the smooth initial data $g \in C^r(\mathbb{R})$ for any integer $r \geq 2$ [23].

Next, we employ the spectral method to discretize the p -domain. We select a sufficiently large domain $p \in [-\pi L, \pi L]$, $L > 0$ such that

$$e^{-\pi L + |\lambda_{\max}(H_1)|T} \approx 0, \quad (20)$$

where $\lambda_{\max}(H_1) = \max_{t \in (0, T)} |\lambda(H_1(t))|$. This ensures that the wave initially supported within the domain remains so throughout the computation. We set the uniform mesh size $\Delta p = 2\pi L/N_p$ where $N_p = 2^{n_p}$ is a positive even integer and grid points denoted by $-\pi L = p_0 < \dots < p_{N_p} = \pi L$. Define the vector \mathbf{w}_h as the collection of the function \mathbf{w} at these grid points by

$$\mathbf{w}_h = \sum_{k \in [N_p]} \sum_{j \in [n]} \mathbf{w}_j(t, p_k) |j\rangle |k\rangle, \quad (21)$$

where \mathbf{w}_j is the j -th component of \mathbf{w} . The one-dimensional basis functions for the Fourier spectral method are typically chosen as

$$\phi_l^p(x) = e^{i\nu_l^p(x+\pi L)}, \quad \nu_l^p = (l - N_p/2)/L, \quad 0 \leq l \leq N_p - 1. \quad (22)$$

Using (22), we define

$$\Phi^p = (\phi_{jl}^p)_{N_p \times N_p} = (\phi_l^p(p_j))_{N_p \times N_p}, \quad D_p = \text{diag}\{\nu_0^p, \dots, \nu_{N_p-1}^p\}. \quad (23)$$

Considering the Fourier spectral discretization on p , one obtains

$$\frac{d}{dt} \mathbf{w}_h = -i(H_1 \otimes P_p) \mathbf{w}_h + i(H_2 \otimes I_{N_p}) \mathbf{w}_h \triangleq -iH_p \mathbf{w}_h. \quad (24)$$

Here P_p is the matrix representation of the momentum operator $-i\partial_p$ and is defined by $P_p = \Phi^p D_p (\Phi^p)^\dagger$.

3.3.1 Turning a non-autonomous system into an autonomous one

In this subsection, we apply the autonomization technique from [10] to transform the time-dependent system into a time-independent one. The approach involves introducing a new variable s , which reformulates the problem as a new system defined in one higher dimension, featuring *time-independent* coefficients, as demonstrated in the following theorem.

Theorem 3.1. *For the non-autonomous system in Equation (29), introduce the following initial-value problem of an autonomous PDE*

$$\frac{d}{dt} \mathbf{v} = -\frac{\partial}{\partial s} \mathbf{v} - iH_p(s) \mathbf{v}, \quad \mathbf{v}(0) = \delta(s) \mathbf{w}_h(0), \quad s \in \mathbb{R}. \quad (25)$$

One can recover $\mathbf{w}_h(t)$ from $\mathbf{v}(t, s)$ using

$$\mathbf{w}_h(t) = \int_{-\infty}^{\infty} \mathbf{v}(t, s) ds. \quad (26)$$

For the discretization in the s domain, we first truncate the infinite s -domain to $[-\pi S, \pi S]$, ensuring that S is sufficiently large so that $e^{-\pi S+T} \approx 0$. This allows us to approximate the problem using periodic boundary conditions. Additionally, we set $H_p(s) = 0$ for $s \leq 0$. We define the collection of the function \mathbf{v} , denoted by \mathbf{v}_h , at the points $-\pi S = s_0 < \dots < s_{N_s} = \pi S$, where $s_i = -\pi S + (i-1)\Delta s$ for $i \in [N_s]$. Here, $N_s = 2^{n_s}$ represents the number of grid points in the s domain, and $\Delta s = \frac{2\pi S}{N_s}$ is the mesh size. Analogous to equations (22)-(23), we define

$$\Phi^s = (\phi_{jl}^s)_{N_s \times N_s} = (e^{i\nu_l^s(s_j + \pi S)})_{N_s \times N_s}, \quad D_s = \text{diag}\{\nu_0^s, \dots, \nu_{N_s-1}^s\}, \quad \nu_l^s = \frac{l - \frac{N_s}{2}}{S},$$

and then

$$P_s = \Phi^s D_s (\Phi^s)^{-1}, \quad H_S = \sum_{l=0}^{N_s-1} (H_1(s_l) \otimes |l\rangle\langle l| \otimes P_p - H_2(s_l) \otimes |l\rangle\langle l| \otimes I_{N_p}).$$

The numerical scheme for the discretization of \mathbf{v} is given by

$$\frac{d}{dt} \mathbf{v}_h = -i(I_n \otimes P_s \otimes I_{N_p} + H_S) \mathbf{v}_h, \quad \mathbf{v}_h(0) = \mathbf{u}_f(0) \otimes \boldsymbol{\delta}_h(0) \otimes \mathbf{g}_h, \quad (27)$$

where $\mathbf{g}_h = [\mathbf{g}(p_0) \dots \mathbf{g}(p_{N_p-1})]^\top$ and $\boldsymbol{\delta}_h = [\delta_h(s_0), \dots, \delta_h(s_{N_s-1})]^\top$. The compactly supported discrete Dirac delta function is defined as

$$\delta_h(s) = \frac{1}{\Delta s} \beta\left(\frac{s}{\Delta s}\right),$$

where $\beta(\xi)$ is the unscaled approximation function supported on the interval $[-q, q]$ for some constant q . We recover the approximation to \mathbf{w}_h , denoted by \mathbf{w}_h^D such that

$$\mathbf{w}_h^D = \Delta s \sum_{l \in [N_s]} (I_n \otimes |l\rangle\langle l| \otimes I_{N_p}) \cdot \mathbf{v}_h. \quad (28)$$

Define

$$H = I_n \otimes P_s \otimes I_{N_p} + \sum_{l \in [N_s]} (H_1(s_l) \otimes |l\rangle\langle l| \otimes D_p - H_2(s_l) \otimes |l\rangle\langle l| \otimes I_{N_p}).$$

By changing variables to $\tilde{\mathbf{v}}_h = [I_n \otimes I_{N_s} \otimes (\Phi^p)^\dagger] \mathbf{v}_h$, one gets

$$\frac{d}{dt} \tilde{\mathbf{v}}_h = -iH \tilde{\mathbf{v}}_h, \quad \tilde{\mathbf{v}}_h(0) = \mathbf{u}_f(0) \otimes \boldsymbol{\delta}_h(0) \otimes \tilde{\mathbf{g}}_h, \quad (29)$$

where $\tilde{\mathbf{g}}_h = (\Phi^p)^\dagger \mathbf{g}_h$. At this point, a quantum simulation can be performed for the Hamiltonian system described by (29). The inverse Quantum Fourier transform is then applied to yield $\mathbf{v}_h = [I_n \otimes I_{N_s} \otimes \Phi^p] \tilde{\mathbf{v}}_h$.

3.3.2 Recovery from Schrödingerisation

Finally, one needs to recover \mathbf{u} from the warped transformation by selecting a suitable domain in p . We adopt the recovery strategy outlined in [21].

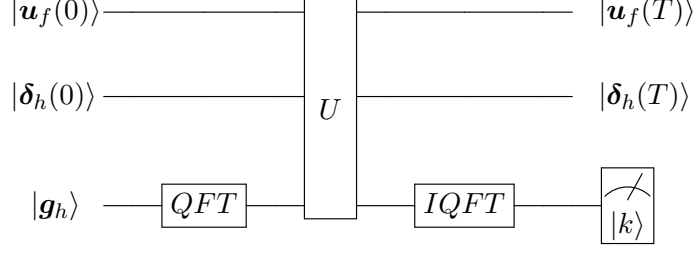


Figure 1: Quantum circuit for Schrödingerisation of Equation (27).

Theorem 3.2. *Assume the eigenvalues of H_1 satisfy $\lambda_1(H_1) \leq \lambda_2(H_1) \cdots \leq \lambda_n(H_1)$, the solution to Equation (16) can be recovered from Equation (19) by*

$$\mathbf{u} = e^{p^*} \mathbf{w}(p^*), \quad \text{for any } p^* > p^\diamond, \quad (30)$$

where $p^\diamond \geq \max\{\lambda_n(H_1)T, 0\}$ with T the stop time of the evolution; or by using the integration,

$$\mathbf{u} = e^{p^*} \int_{p^*}^{\infty} \mathbf{w}(q) dq, \quad p^* > p^\diamond. \quad (31)$$

In the case of Equation (15), we have $|\lambda(H_1)| \leq \frac{1}{2}$, the numerical electromagnetic field is recovered by

$$\begin{aligned} \mathbf{u}_h|k\rangle &= e^{p_k} (I_n \otimes |k\rangle\langle k|) \mathbf{w}_h^D \\ &= e^{p_k} \Delta s (I_n \otimes |k\rangle\langle k|) \sum_{l \in [N_s]} (I_n \otimes \langle l| \times I_{N_p}) \mathbf{v}_h \\ &= e^{p_k} \Delta s \sum_{l \in [N_s]} (I_n \otimes \langle l| \otimes I_{N_p}) M_k \mathbf{v}_h \quad p_k > T/2, \end{aligned} \quad (32)$$

where $M_k = I_{n \times N_s} \otimes |k\rangle\langle k|$ is the projection measurement operator. Here we remark that we use the quantum computer to evaluate

$$\mathbf{v}_h = (I_n \otimes I_{N_s} \otimes \Phi^p) U (I_n \otimes I_{N_s} \otimes (\Phi^p)^\dagger) (\mathbf{u}_f(0) \otimes \boldsymbol{\delta}_h(0) \otimes \mathbf{g}_h) \triangleq \mathcal{U} \mathbf{v}_h(0),$$

where $U = \exp(-iHT)$ is unitary and $\mathcal{U} = (I_n \otimes I_{N_s} \otimes \Phi^p) U (I_n \otimes I_{N_s} \otimes (\Phi^p)^\dagger)$. A measurement corresponding to the projection $M_k = I_n \otimes I_{N_s} \otimes |k\rangle\langle k|$ is performed to select the $|k\rangle$ component of the state $|\mathbf{v}_h\rangle$. Following the measurement, the summation is executed on a classical computer. The complete circuit for implementing the quantum simulation of $|\mathbf{v}_h\rangle$ is illustrated in Figure 1, where QFT (IQFT) denotes the (inverse) quantum Fourier transform.

3.4 A higher order improvement in the extended domains

In order to achieve r -th order convergence rates of spectral methods and r -th order approximation to the delta function, it is essential that $\beta(\xi) \in H^r(\mathbb{R})$ is sufficiently smooth and fulfills the condition

$$\left| \Delta s \sum_{l \in [N_s]} \delta_h(s_l - s) f(s_l) - f(s) \right| \leq C \Delta s^r \quad (33)$$

for $f(x) \in C^r(\mathbb{R})$ [42]. Additionally, the initial data in the extended domain $g(p) \in C^r(\mathbb{R})$ should exhibit sufficient smoothness to ensure that $\mathbf{w}_h(p, t) \in C^r(\mathbb{R})$. Then, we use the construction

in [29, Appendix] to obtain r -th order approximation to the delta function $\beta(\xi) \in H^r(\mathbb{R})$. As an example, we present the 3rd-order interpolating function $\beta(\xi) \in H^2(\mathbb{R})$ from [48], given by

$$\beta(\xi) = \begin{cases} 1 - \frac{5}{2}|x|^2 + \frac{3}{2}|x|^3, & 0 \leq |x| \leq 1, \\ \frac{1}{2}(2 - |x|)^2(1 - |x|), & 1 \leq |x| \leq 2, \\ 0, & \text{otherwise.} \end{cases} \quad (34)$$

Meanwhile we choose $g(p) \in C^2(\mathbb{R})$ in [23]:

$$g(p) = \begin{cases} (\frac{19}{2} - \frac{19}{2}e^{-1})p^5 + (\frac{49}{2} - 23e^{-1})p^4 + (\frac{35}{2} - \frac{29}{2}e^{-1})p^3 + \frac{1}{2}p^2 - p + 1 & p \in (-1, 0), \\ e^{-|p|} & p \in (-\infty, -1] \cup [0, \infty). \end{cases} \quad (35)$$

For general r , this will lead to essentially the spectral accuracy for the approximation in the extended space, if a spectral method is used [23].

4 Quantum circuit for Maxwell's equations

The complete circuit for implementing the Schrödingerization method for Maxwell's equations is presented in Figure 1. In this section, we focus on the detailed construction of the quantum circuit for the unitary operation

$$U = \exp(-iHT) = \exp(-i(I_n \otimes P_s \otimes I_{N_p} + H_S)T).$$

According to Equation (10), we define

$$\mathbf{J}_{\alpha h} = \sum_j \frac{J_{\alpha, j}}{c_0} |j\rangle, \quad \alpha = x, y, z, \rho,$$

where $J_{\rho, j} = \rho_j$. For simplicity, we make the following assumptions.

Assumption 4.1. For the parameter s_l , $0 \leq s_l < T$, $l \in \mathcal{I}_s$ with $|\mathcal{I}_s| \leq \mathcal{O}(n_s)$, the discretization source term $\mathbf{J}_{\alpha h}^l = \mathbf{J}_{\alpha h}(s_l)$ takes the value either $J_{\alpha, 1}^l$, or $J_{\alpha, 0}^l$, such that

$$\mathbf{J}_{\alpha h, j}^l = \begin{cases} J_{\alpha, 1}^l & \text{for } j \in \mathcal{I}_\alpha^l, \\ J_{\alpha, 0}^l & \text{otherwise,} \end{cases} \quad \alpha = x, y, z, \rho.$$

In addition, $\mathbf{J}_{\alpha, h}^l \equiv 0$ for $l \in [N_s] \setminus \mathcal{I}_s$, and we have $|\mathcal{I}_\alpha^l| = \max_{l \in \mathcal{I}_s} |\mathcal{I}_\alpha^l| \leq \mathcal{O}(m)$.

To simplify notation, we denote

$$\Theta_j = \sigma_{j_{3m-1}j_{3m-2}} \otimes \cdots \otimes \sigma_{j_0j_1}, \quad 0 \leq j \leq 2^{3m} - 1, \quad (36)$$

where $j = (j_{3m-1} \cdots j_0) = \sum_{i=0}^{3m-1} j_i 2^i$, $j_i \in \{0, 1\}$ is the binary representation of j . By introducing

$$\begin{aligned} \mathbf{F}^\alpha(s_l) &= \sum_{j \in \mathcal{I}_\alpha^l} \frac{1}{c_0} (J_{\alpha, 1}^l - J_{\alpha, 0}^l) |j\rangle \langle j| + \frac{J_{\alpha, 0}^l}{c_0} \mathbf{1}^{\otimes 3m} \\ &= \sum_{j \in \mathcal{I}_\alpha^l} \frac{1}{c_0} (J_{\alpha, 1}^l - J_{\alpha, 0}^l) \Theta_j + \frac{J_{\alpha, 0}^l}{c_0} \mathbf{1}^{\otimes 3m}, \quad \alpha = x, y, z, \rho, \end{aligned} \quad (37)$$

one has the formula of \mathbf{F} as

$$\mathbf{F}(s_l) = \sigma_{3,x} \otimes \mathbf{F}^x(s_l) + \sigma_{3,y} \otimes \mathbf{F}^y(s_l) + \sigma_{3,z} \otimes \mathbf{F}^z(s_l) + \sigma_{3,\rho} \otimes \mathbf{F}^\rho(s_l), \quad (38)$$

with $\sigma_{3,x} = \sigma_{00}^{\otimes 3}$, $\sigma_{3,y} = \sigma_{00}^{\otimes 2} \otimes \sigma_{11}$, $\sigma_{3,z} = \sigma_{00} \otimes \sigma_{11} \otimes \sigma_{00}$, $\sigma_{3,\rho} = \sigma_{11}^{\otimes 3}$.

We note that by employing the autonomosization technique described in [10], we can transform the time evolution of the Hamiltonian system into a spatial variable-coefficient Schrödinger-type equation. Consequently, constructing the circuit diagram for the time evolution of the Hamiltonian system essentially involves creating a quantum circuit for variable-coefficient unitary operators. For more general cases of variable-coefficient matrices, we refer to [35, 36].

The essential aspect of constructing the circuit lies in implementing the quantum circuit for the Hamiltonian operator $U(\tau) = \exp(iH\tau)$, where τ represents the time increment. This can be achieved by applying the first-order Lie-Trotter-Suzuki decomposition. Given that the Hamiltonian H can be expressed as

$$H = H_{D_s} + H_F + H_{\text{curl}}, \quad H_{D_s} = \mathbf{1}^{\otimes(3m+4)} \otimes P_s \otimes \mathbf{1}^{\otimes n_p}, \quad (39)$$

$$H_F = \frac{1}{2} \sum_{l=0}^{N_s-1} (X \otimes \mathbf{F}(s_l) \otimes |l\rangle\langle l| \otimes D_p - Y \otimes \mathbf{F}(s_l) \otimes |l\rangle\langle l| \otimes \mathbf{1}^{\otimes n_p}), \quad (40)$$

$$H_{\text{curl}} = i(\sigma_{00} \otimes \sigma_{01} \otimes M_{\nabla_h \times}^E + \sigma_{00} \otimes \sigma_{10} \otimes M_{\nabla_h \times}^B) \otimes \mathbf{1}^{\otimes(n_p+n_s)}, \quad (41)$$

we introduce the operators

$$\mathcal{U}_1(\tau) = \exp(-iH_{D_s}\tau), \quad \mathcal{U}_2(\tau) = \exp(-iH_F\tau), \quad \mathcal{U}_3(\tau) = \exp(-iH_{\text{curl}}\tau). \quad (42)$$

Thus, the approximation for $U(\tau)$ can be formulated as

$$\exp(-iH\tau) \approx \mathcal{U}_1(\tau)\mathcal{U}_2(\tau)\mathcal{U}_3(\tau). \quad (43)$$

4.1 Quantum circuit for $\mathcal{U}_1(\tau)$

From the definition of P_s , it is easy to construct the circuit of \mathcal{U}_1 as follows

$$\begin{aligned} \mathcal{U}_1(\tau) &= \exp(-i\mathbf{1}^{\otimes 3m+4} \otimes \Phi^s D_s (\Phi^s)^\dagger \otimes \mathbf{1}^{\otimes n_p}) \\ &= \mathbf{1}^{\otimes(3m+4)} \otimes \left(\Phi^s \exp\left(\frac{-i\tau}{2S} \sum_{l \in [N_s]} \left(l - \frac{N_s}{2}\right) |l\rangle\langle l|\right) (\Phi^s)^\dagger \right) \\ &= \mathbf{1}^{\otimes(3m+4)} \otimes \left(\Phi^s \left(\exp\left(\frac{i\tau N_s}{4S}\right) \mathbf{1}^{\otimes n_s} \right) \cdot \left(\exp\left(\frac{-i\tau}{2S} \sum_{l \in [N_s]} l |l\rangle\langle l|\right) (\Phi^s)^\dagger \right) \right) \otimes \mathbf{1}^{\otimes n_p} \\ &\triangleq \mathbf{1}^{\otimes(3m+4)} \otimes \tilde{\mathcal{U}}_1(\tau) \otimes \mathbf{1}^{\otimes n_p}. \end{aligned} \quad (44)$$

Using the binary representation of integers $l = (l_{n_s-1} \cdots l_0) = \sum_{j=0}^{n_s-1} l_j 2^j$, $l_j \in \{0, 1\}$, one gets

$$\exp\left(\frac{-i\tau}{2S} \sum_{l \in [N_s]} l |l\rangle\langle l|\right) = \bigotimes_{j=0}^{n_s-1} \sum_{l_j=0,1} e^{-\frac{i\tau}{2S} 2^j \sigma_{l_j}} = \bigotimes_{j=0}^{n_s-1} P\left(\frac{-2^j-1}{S} \tau\right), \quad (45)$$

where $P(\theta) = \begin{bmatrix} 1 & 0 \\ 0 & e^{i\theta} \end{bmatrix}$ is the phase gate. According to Equation (44) and (45), one gets the circuit of $\tilde{\mathcal{U}}_1(\tau)$ as shown in Figure 2.

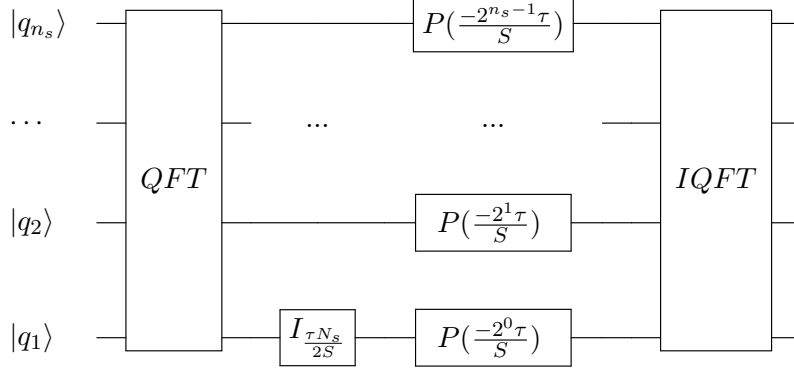


Figure 2: Quantum circuit for the operator $\tilde{\mathcal{U}}_1(\tau)$, where $I_\theta = R_z(-\theta)P(\theta)$.

4.2 Quantum circuits for $\mathcal{U}_2(\tau)$

For any fixed $l = (l_{n_s} \cdots l_0) \in \mathcal{I}_s$ and $j = (j_{3m-1} \cdots j_0) \in \mathcal{I}_\alpha^l$, according to the notation in Equation (36) and the representation of spatial variable coefficient matrix in Equation (37), we define

$$H_{X_p, l_j}^\alpha = \frac{1}{2c_0} (J_{\alpha,1}^l - J_{\alpha,0}^l) X \otimes \sigma_{3,\alpha} \otimes \Theta_j \otimes \Theta_l \otimes D_p, \quad (46)$$

$$H_{X_p, l}^\alpha = \frac{1}{2c_0} J_{\alpha,0}^l X \otimes \sigma_{3,\alpha} \otimes \mathbf{1}^{\otimes 3m} \otimes \Theta_l \otimes D_p, \quad (47)$$

$$H_{Y_p, l_j}^\alpha = \frac{1}{2c_0} (J_{\alpha,0}^l - J_{\alpha,1}^l) Y \otimes \sigma_{3,\alpha} \otimes \Theta_j \otimes \Theta_l \otimes \mathbf{1}^{\otimes n_p}, \quad (48)$$

$$H_{Y_p, l}^\alpha = \frac{1}{2c_0} (-J_{\alpha,0}^l) Y \otimes \sigma_{3,\alpha} \otimes \mathbf{1}^{\otimes (3m)} \otimes \Theta_l \otimes \mathbf{1}^{\otimes n_p}. \quad (49)$$

Then one can rewrite H_F as

$$H_F = \sum_{\alpha=x,y,z,\rho} \sum_{l \in \mathcal{I}_s} \sum_{j \in \mathcal{I}_\alpha^l} (H_{X_p, l_j}^\alpha + H_{Y_p, l_j}^\alpha) + H_{X_p, l}^\alpha + H_{Y_p, l}^\alpha. \quad (50)$$

Using Trotter's splitting, one has

$$\mathcal{U}_2(\tau) \approx \prod_{\alpha=x,y,z,\rho} \prod_{l \in \mathcal{I}_s} \prod_{j \in \mathcal{I}_\alpha^l} \mathcal{U}_{X_p, l_j}^\alpha \cdot \mathcal{U}_{Y_p, l_j}^\alpha \cdot \mathcal{U}_{X_p, l}^\alpha \cdot \mathcal{U}_{Y_p, l}^\alpha \triangleq \mathcal{V}_2(\tau), \quad (51)$$

where

$$\mathcal{U}_{\beta, l_j}^\alpha = \exp(-iH_{\beta, l_j}^\alpha \tau), \quad \mathcal{U}_{\beta, l}^\alpha = \exp(-iH_{\beta, l}^\alpha \tau), \quad \beta = \{X_p, Y_p\}.$$

Define a multi-controlled $RX(\theta)$ gate acting on the $(m+1)$ -th qubit. This gate becomes active when the qubits indexed in \mathcal{I}^1 are all set to 1 and the qubits indexed in \mathcal{I}^0 are all set to 0, denoted

$$\text{CRX}_{m+1}^{\mathcal{I}^1, \mathcal{I}^0}(2\theta) = \exp(-i\theta X \otimes \tilde{\sigma}_{j_{m-1}j_{m-1}} \otimes \cdots \otimes \tilde{\sigma}_{j_0j_0}), \quad (52)$$

where $\tilde{\sigma}_{j_k}$, $k \in [m]$ is determined by

$$\tilde{\sigma}_{j_k j_k} = \begin{cases} \sigma_{00} & k \in \mathcal{I}^0, \\ \sigma_{11} & k \in \mathcal{I}^1, \\ \mathbf{1} & \text{otherwise.} \end{cases}$$

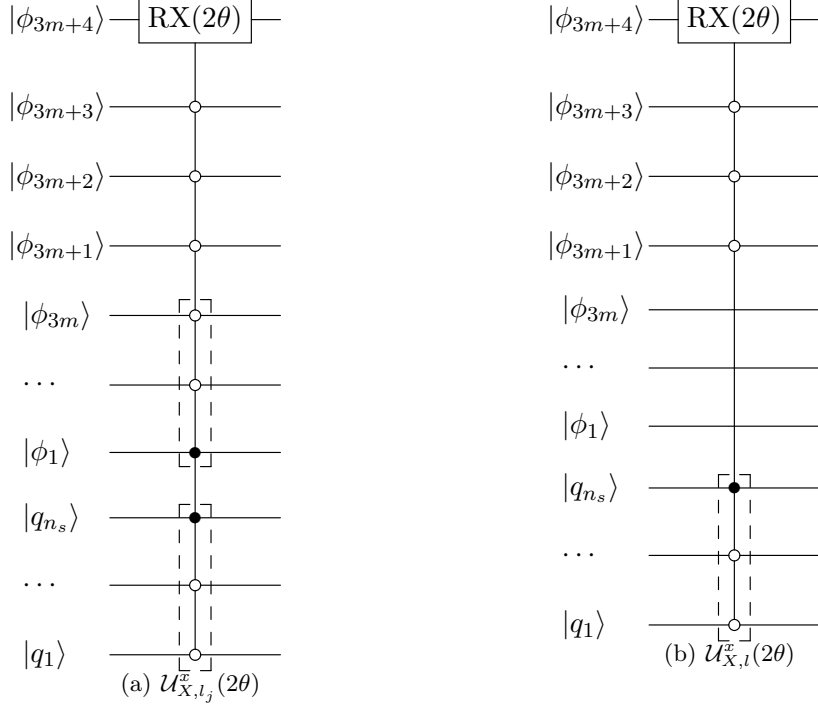


Figure 3: Quantum circuit for $\mathcal{U}_{X,l_j}^x(2\theta)$ and $\mathcal{U}_{X,l}^x(2\theta)$ with $\mathcal{I}_{j,3m}^1 = \{0\}$, $\mathcal{I}_{l,n_s}^1 = \{n_s - 1\}$.

Similarly, we can define $\text{CRY}_{m+1}^{\mathcal{I}^1, \mathcal{I}^0}(2\theta)$ and $\text{CRZ}_{m+1}^{\mathcal{I}^1, \mathcal{I}^0}(2\theta)$. For the fixed $l = (l_{n_s} \cdots l_0) \in \mathcal{I}_s$ and $j = (j_{3m-1} \cdots j_0) \in \mathcal{I}_\alpha^l$, the index sets for control points are defined by

$$\mathcal{I}_{j,3m}^i = \{k \in [3m] : j_k = i\}, \quad \mathcal{I}_{l,n_s}^i = \{k \in [n_s] : l_k = i\}, \quad i = 0, 1. \quad (53)$$

Using the definition provided in (52), we define the operators corresponding to the circuits shown in Figure 3 as follows

$$\mathcal{U}_{X,l_j}^\alpha(2\theta) = \exp(-i\theta X \otimes \sigma_{3,\alpha} \otimes \Theta_j \otimes \Theta_l) = \text{CRX}_{3m+4+n_s}^{\mathcal{I}_{\alpha,1}^1, \mathcal{I}_{\alpha,1}^0}(2\theta) \quad \alpha = x, y, z, \rho, \quad (54)$$

$$\mathcal{U}_{X,l}^\alpha(2\theta) = \exp(-i\theta X \otimes \sigma_{3,\alpha} \otimes \mathbf{1}^{\otimes 3m} \otimes \Theta_l) = \text{CRX}_{3m+4+n_s}^{\mathcal{I}_{\alpha,0}^1, \mathcal{I}_{\alpha,0}^0}(2\theta) \quad \alpha = x, y, z, \rho. \quad (55)$$

Here, the sets $\mathcal{I}_{\alpha,1}^k$ and $\mathcal{I}_{\alpha,0}^k$ are defined as

$$\begin{aligned} \mathcal{I}_{\alpha,1}^k &= \{n_s + 3m + \mathcal{I}_\alpha^k\} \cup \{n_s + \mathcal{I}_{j,3m}^k\} \cup \mathcal{I}_{l,n_s}^k, \\ \mathcal{I}_{\alpha,0}^k &= \{n_s + 3m + \mathcal{I}_\alpha^k\} \cup \mathcal{I}_{l,n_s}^k, \end{aligned}$$

for $k = 0, 1$. The sets $\mathcal{I}_{j,3m}^k, \mathcal{I}_{l,n_s}^k$ are defined in (53). Additionally, we have

$$\mathcal{I}_x^1 = \emptyset, \quad \mathcal{I}_y^1 = \{0\}, \quad \mathcal{I}_z^1 = \{1\}, \quad \mathcal{I}_\rho^1 = \{0, 1, 2\}, \quad \mathcal{I}_\alpha^0 = \{0, 1, 2\} \setminus \mathcal{I}_\alpha^1, \quad \alpha = x, y, z, \rho,$$

as determined by the definition of $\sigma_{3,\alpha}$. The circuit of $\mathcal{U}_{X,l_j}^\alpha(2\theta)$ and $\mathcal{U}_{X,l}^\alpha(2\theta)$ are shown in Figure 3. Similarly, one has $\mathcal{U}_{Y,l_j}^\alpha(2\theta)$ and $\mathcal{U}_{Y,l}^\alpha(2\theta)$. Thus, it yields

$$\mathcal{U}_{Y_p,l_j}^\alpha = \mathcal{U}_{Y,l_j}^\alpha(\theta_l^{\alpha,1} \tau) \otimes \mathbf{1}^{\otimes n_p}, \quad \mathcal{U}_{Y_p,l}^\alpha = \mathcal{U}_{Y,l}^\alpha(\theta_l^{\alpha,0} \tau) \otimes \mathbf{1}^{\otimes n_p}, \quad (56)$$

where $\theta_l^{\alpha,1} = \frac{J_{\alpha,0}^l - J_{\alpha,1}^l}{c_0}$, $\theta_l^{\alpha,0} = -\frac{J_{\alpha,0}^l}{c_0}$.

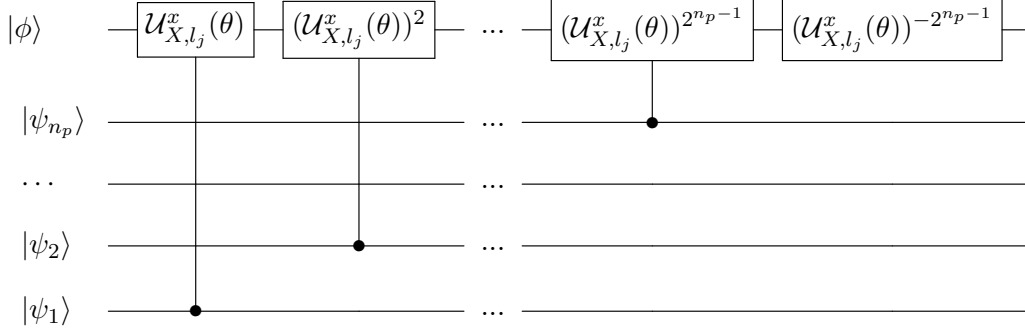


Figure 4: Quantum circuit for \mathcal{U}_{X_p, l_j}^x with $\theta = \tau\theta_{l_p}^{\alpha, 1}$.

Noting that $D_p = \sum_{k=0}^{N_p-1} \frac{1}{L} (k - \frac{N_p}{2}) |k\rangle\langle k|$, one gets the expression of $\mathcal{U}_{X_p, l_j}^\alpha$, $\mathcal{U}_{X_p, l}^\alpha$ as follows

$$\begin{aligned} \mathcal{U}_{X_p, l_j}^\alpha &= \left(\sum_{k \in [N_p]} \mathcal{U}_{X_p, l_j}^\alpha(k\tau\theta_{l_p}^{\alpha, 1}) \otimes |k\rangle\langle k| \right) \left(\mathcal{U}_{X_p, l_j}^\alpha(-N_p\tau\theta_{l_p}^{\alpha, 1}) \otimes \mathbf{1}^{\otimes n_p} \right), \\ \mathcal{U}_{X_p, l}^\alpha &= \left(\sum_{k \in [N_p]} \mathcal{U}_{X_p, l}^\alpha(k\tau\theta_{l_p}^{\alpha, 0}) \otimes |k\rangle\langle k| \right) \left(\mathcal{U}_{X_p, l}^\alpha(-N_p\tau\theta_{l_p}^{\alpha, 0}) \otimes \mathbf{1}^{\otimes n_p} \right), \end{aligned}$$

where $\theta_{l_p}^{\alpha, 1} = \frac{1}{Lc_0} (J_{\alpha, 0}^l - J_{\alpha, 1}^l)$ and $\theta_{l_p}^{\alpha, 0} = \frac{J_{\alpha, 0}^l}{2Lc_0}$. Using the binary representation of integers $k = (k_{n_p-1} \cdots k_0) = \sum_{g=0}^{n_p-1} 2^g k_g$, $k_g \in \{0, 1\}$, one gets

$$\mathcal{U}_{X_p, l_j}^\alpha(k\theta) = (\mathcal{U}_{X_p, l_j}^\alpha(\theta))^k = \prod_{g=0}^{n_p-1} (\mathcal{U}_{X_p, l_j}^\alpha(\theta))^{k_g 2^g}.$$

Therefore, there holds

$$\begin{aligned} \sum_{k \in [N_p]} \mathcal{U}_{X_p, l_j}^\alpha(k\tau\theta_{l_p}^{\alpha, 1}) \otimes |k\rangle\langle k| &= \sum_{k_{n_p}, \dots, k_0} \prod_{g=0}^{n_p-1} (\mathcal{U}_{X_p, l_j}^\alpha(\tau\theta_{l_p}^{\alpha, 1}))^{k_g 2^g} \otimes (\sigma_{k_{n_p} k_{n_p}} \otimes \cdots \otimes \sigma_{k_0 k_0}) \\ &= \prod_{g=0}^{n_p-1} \left(\sum_{k_g=0,1} (\mathcal{U}_{X_p, l_j}^\alpha(\tau\theta_{l_p}^{\alpha, 1}))^{k_g 2^g} \otimes \sigma_{k_g k_g} \right) \\ &= \prod_{g=0}^{n_p-1} \left((\mathcal{U}_{X_p, l_j}^\alpha(\tau\theta_{l_p}^{\alpha, 1}))^{k_g 2^g} \otimes |1\rangle\langle 1| + \mathbf{1}^{\otimes 3m+4+n_s} \otimes |0\rangle\langle 0| \right). \end{aligned} \quad (57)$$

The product \prod denotes the regular matrix product for the first register, which consists of n_s+3m+4 qubits, and the tensor product for the second register. Since $(\mathcal{U}_{X_p, l_j}^\alpha(\theta))^{2^g}$ can be implemented at a cost independent of g , the advantage of applying the binary representation of k can be realized. The circuit for $\mathcal{U}_{X_p, l_j}^\alpha$ is illustrated in Figure 4. The circuit for $\mathcal{U}_{X_p, l}^\alpha$ is obtained by replacing $\mathcal{U}_{X_p, l_j}^\alpha$ with $\mathcal{U}_{X_p, l}^\alpha$, as shown in Figure 5.

4.3 Quantum circuit for $\mathcal{U}_3(\tau)$

Before giving the specific circuit for $\mathcal{U}_3(\tau)$, we use the Bell basis to decompose a class of the matrix shown in [16].

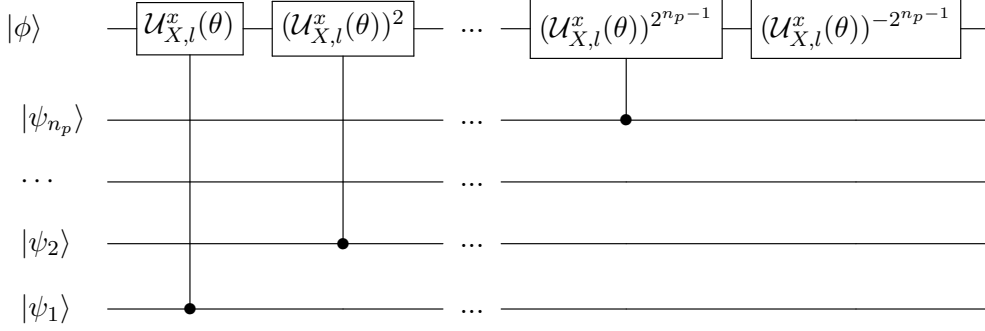


Figure 5: Quantum circuit for $\mathcal{U}_{X,l}^x$ with $\theta = \tau\theta_l^{\alpha,1}$.

Lemma 4.1. *Given an operator of the form $S = e^{i\lambda}\sigma_{01} \otimes \sigma_{10}^{\otimes(n-1)} + e^{-i\lambda}\sigma_{10} \otimes \sigma_{01}^{\otimes(n-1)}$, where λ is a real number, there exists a unitary matrix U such that*

$$S = U_n^{\mathcal{I}}(-\lambda)\Lambda(U_n^{\mathcal{I}}(\lambda))^\dagger,$$

where $\Lambda = Z \otimes \sigma_{11}^{\otimes(n-1)}$. The unitary matrix $U_n^{\mathcal{I}}(-\lambda)$ is defined as

$$U_n^{\mathcal{I}}(-\lambda) = \left(\prod_{k \in \mathcal{I}} \text{CNOT}_k^n \right) P_n(\lambda) H_n,$$

where $\mathcal{I} = \{1, 2, \dots, n-1\}$ is the index set, H_n is the Hadamard gate acting on the n -th qubit, $P_n(\lambda)$ is the phase gate $P(\lambda)$ acting on the n -th qubit and CNOT_k^n is the CNOT gate acting on the k -th qubit controlled by the n -th qubit.

To present the explicit quantum circuit for \mathcal{U}_3 , we first decompose H_{curl} into

$$\begin{aligned} H_{\text{curl}} &= i(\sigma_{00} \otimes \sigma_{01} \otimes M_{\nabla_{h \times}}^E + \sigma_{00} \otimes \sigma_{10} \otimes M_{\nabla_{h \times}}^B) \otimes \mathbf{1}^{\otimes(n_p+n_s)} \\ &= (H_x + H_y + H_z) \otimes \mathbf{1}^{\otimes(n_s+n_p)}, \end{aligned} \quad (58)$$

where the matrices H_x , H_y and H_z are defined as follows

$$\begin{aligned} H_x &= (\sigma_{00} \otimes \sigma_{01} \otimes Y \otimes X \otimes D_x^+ - \sigma_{00} \otimes \sigma_{10} \otimes Y \otimes X \otimes D_x^-), \\ H_y &= -(\sigma_{00} \otimes \sigma_{01} \otimes Y \otimes Z \otimes D_y^+ - \sigma_{00} \otimes \sigma_{10} \otimes Y \otimes Z \otimes D_y^-), \\ H_z &= (\sigma_{00} \otimes \sigma_{01} \otimes \mathbf{1} \otimes Y \otimes D_z^+ - \sigma_{00} \otimes \sigma_{10} \otimes \mathbf{1} \otimes Y \otimes D_z^-). \end{aligned}$$

The circuit for \mathcal{U}_3 is approximated by $\mathcal{U}_3 \approx (\mathcal{U}_x \mathcal{U}_y \mathcal{U}_z) \otimes \mathbf{1}^{\otimes(n_s+n_p)}$ with

$$\mathcal{U}_x = \exp(-iH_x\tau), \quad \mathcal{U}_y = \exp(-iH_y\tau), \quad \mathcal{U}_z = \exp(-iH_z\tau).$$

From Equations (5) and (6), we find that $H_x = H_{x_1} + H_{x_2}$, where H_{x_1} and H_{x_2} can be defined by

$$\begin{aligned} H_{x_1} &= -\left(\frac{1}{\Delta x} \sigma_{00} \otimes \sigma_{01} \otimes Y \otimes X \otimes \sum_{j=1}^m \mathbf{1}^{\otimes(3m-j)} \otimes \sigma_{10} \otimes \sigma_{01}^{\otimes(j-1)} \right. \\ &\quad \left. + \frac{1}{\Delta x} \sigma_{00} \otimes \sigma_{10} \otimes Y \otimes X \otimes \sum_{j=1}^m \mathbf{1}^{\otimes(3m-j)} \otimes \sigma_{01} \otimes \sigma_{10}^{\otimes(j-1)} \right), \\ H_{x_2} &= \frac{1}{\Delta x} \sigma_{00} \otimes X \otimes Y \otimes X \otimes \mathbf{1}^{\otimes 2m} \otimes \mathbf{I}^r. \end{aligned}$$

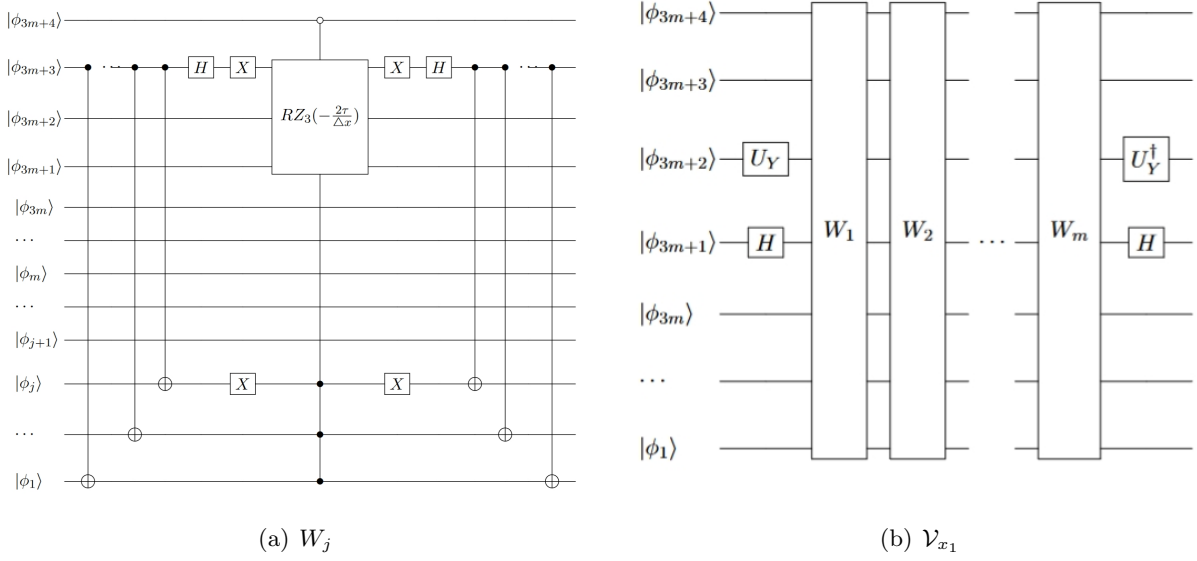


Figure 6: Quantum circuit for W_j and \mathcal{V}_{x_1} .

We can express the tensor product of the Pauli matrices by

$$Z \otimes Y \otimes X = (\mathbf{1} \otimes U_Y \otimes H) \cdot Z_{\sigma,3} \cdot (\mathbf{1} \otimes U_Y^\dagger \otimes H), \quad (59)$$

$$X \otimes Y \otimes X = (H \otimes U_Y \otimes H) \cdot Z_{\sigma,3} \cdot (H \otimes U_Y^\dagger \otimes H). \quad (60)$$

Here U_Y is defined as $HP(\frac{\pi}{2})H$ and $Z_{\sigma,3}$ represents $Z^{\otimes 3}$. Applying Lemma 4.1 yields

$$H_{x_1} = \tilde{U}_{ZYX} \cdot \sum_{j=1}^m \left(U_{3m+3}^{\mathcal{I}_{x,j}}(0) X_{3m+3,j} (\sigma_{00} \otimes \frac{-Z_{\sigma,3}}{\Delta x} \otimes \mathbf{1}^{\otimes(3m-j)} \otimes \sigma_{11}^{\otimes j}) X_{3m+3,j} (U_{3m+3}^{\mathcal{I}_{x,j}}(0))^\dagger \right) \tilde{U}_{ZYX}^\dagger.$$

In this expression, \tilde{U}_{ZYX} is defined as $\mathbf{1}^{\otimes 2} \otimes U_Y \otimes H \otimes \mathbf{1}^{\otimes 3m}$. The term $U_{3m+3}^{\mathcal{I}_{x,j}}(\lambda)$ is given by $(\prod_{k \in \mathcal{I}_{x,j}} \text{CNOT}_k^{3m+3}) P_{3m+3}(\lambda) H_{3m+3}$. The set $\mathcal{I}_{x,j}$ represents $\{1, 2, \dots, j\}$, and $X_{3m+3,j}$ denotes the X gate acting on the $(3m+3)$ -th and j -th qubit. Using the first-order Lie-Trotter-Suzuki decomposition, it yields

$$\begin{aligned} \mathcal{U}_{x_1} &= \exp(-iH_{x_1}\tau) \\ &\approx \tilde{U}_{ZYX} \cdot \prod_{j=1}^m \left(U_{3m+3}^{\mathcal{I}_{x,j}}(0) X_{3m+3,j} \text{CRZ}_{3m+1 \rightarrow 3m+3}^{\mathcal{I}_{x,j}^1, \mathcal{I}_{x,j}^0} \left(\frac{-2\tau}{\Delta x} \right) X_{3m+3,j} (U_{3m+3}^{\mathcal{I}_{x,j}}(0))^\dagger \right) \cdot \tilde{U}_{ZYX}^\dagger \\ &= \tilde{U}_{ZYX} \prod_{j=1}^m W_j \tilde{U}_{ZYX}^\dagger = \mathcal{V}_{x_1}. \end{aligned}$$

Here, $\text{CRZ}_{3m+1 \rightarrow 3m+3}^{\mathcal{I}_{x,j}^1, \mathcal{I}_{x,j}^0}(2\theta)$ represents a multi-gate $\text{RZ}_3(2\theta) = \exp(-i\theta Z_{\sigma,3})$, acting on the $(3m+1)$ to $(3m+3)$ -th qubits controlled by $\mathcal{I}_{x,j}^1$ and $\mathcal{I}_{x,j}^0$ given by

$$\mathcal{I}_{x,j}^1 = \{1, 2, \dots, j\}, \quad \mathcal{I}_{x,j}^0 = \{3m+4\}.$$

The circuits of W_j and \mathcal{V}_{x_1} are shown in Figure 6. Noting that $\mathbf{I}^r = \mathbf{1}^{\otimes m} - \sigma_{00}^{\otimes m}$ and Equation

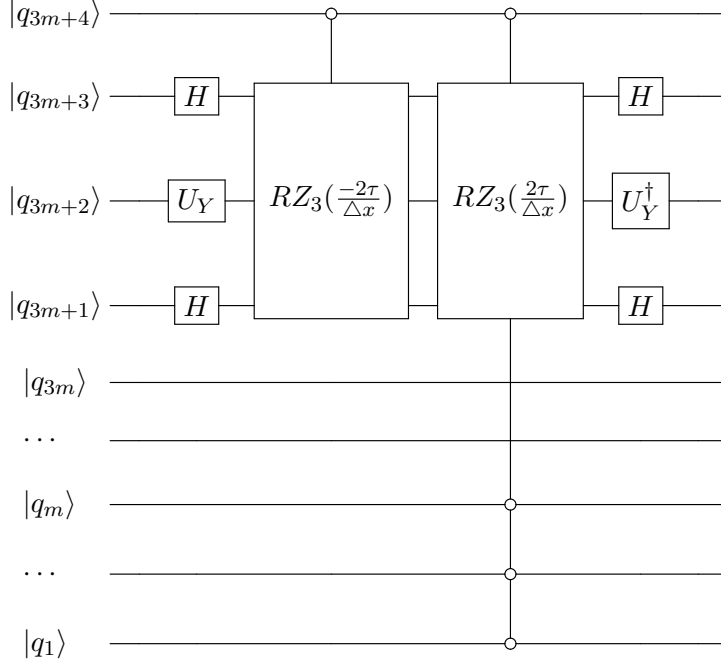


Figure 7: Quantum circuit for \mathcal{U}_{x_2} .

(60), one has

$$\begin{aligned} \mathcal{U}_{x_2} &= \exp(-iH_{x_2}\tau) \\ &= \tilde{U}_{XYX} \cdot \text{CRZ}_{\sigma_{3m+1 \rightarrow 3m+3}}^{\emptyset, \{3m+4\}}\left(\frac{-2\tau}{\Delta x}\right) \cdot \text{CRZ}_{\sigma_{3m+1 \rightarrow 3m+3}}^{\emptyset, \{1, 2, \dots, m, 3m+4\}}\left(\frac{2\tau}{\Delta x}\right) \cdot \tilde{U}_{XYX}^\dagger, \end{aligned}$$

where $\tilde{U}_{XYX} = \mathbf{1} \otimes H \otimes U_Y \otimes H \otimes \mathbf{1}^{\otimes 3m}$. The circuit of \mathcal{U}_{x_2} is shown in Figure 7, and the approximation of \mathcal{U}_x is given by

$$\mathcal{U}_x = \mathcal{U}_{x_1} \mathcal{U}_{x_2} \approx \mathcal{V}_x = \mathcal{V}_{x_1} \cdot \mathcal{U}_{x_2}. \quad (61)$$

An argument similar to the computation of \mathcal{U}_x shows the approximation of \mathcal{U}_y as

$$\mathcal{U}_y \approx \mathcal{V}_y = \mathcal{V}_{y_1} \cdot \mathcal{U}_{y_2}, \quad (62)$$

$$\mathcal{V}_{y_1} = \tilde{U}_{YZZ} \cdot \prod_{j=1}^m \left(U_{3m+3}^{\mathcal{I}_{y,j}}(0) X_{3m+3,j} \text{CRZ}_{3m+1 \rightarrow 3m+3}^{\mathcal{I}_{y,j}^1, \mathcal{I}_{y,j}^0} \left(\frac{2\tau}{\Delta y} \right) X_{3m+3,j} (U_{3m+3}^{\mathcal{I}_{y,j}}(0))^\dagger \right) \cdot \tilde{U}_{YZZ}^\dagger,$$

$$\mathcal{U}_{y_2} = \tilde{U}_{XYZ} \cdot \text{CRZ}_{3m+1 \rightarrow 3m+3}^{\emptyset, \{3m+4\}} \left(\frac{2\tau}{\Delta y} \right) \cdot \text{CRZ}_{3m+1 \rightarrow 3m+3}^{\emptyset, \{m+1, \dots, 2m, 3m+4\}} \left(\frac{-2\tau}{\Delta y} \right) \cdot \tilde{U}_{XYZ}^\dagger,$$

where $\mathcal{I}_{y,j} = \{m+1, m+2, \dots, m+j\}$, and

$$\mathcal{I}_{y,j}^0 = \{3m+4\}, \quad \mathcal{I}_{y,j}^1 = \{m+1, m+2, \dots, m+j\}.$$

Here $\tilde{U}_{YZZ} = \mathbf{1}^{\otimes 2} \otimes U_Y \otimes \mathbf{1}^{\otimes (3m+1)}$, and $\tilde{U}_{XYZ} = \mathbf{1} \otimes H \otimes U_Y \otimes \mathbf{1}^{\otimes (3m+1)}$. Similarly, one has the approximation of circuit of \mathcal{U}_z shown as

$$\mathcal{U}_z \approx \mathcal{V}_z = \mathcal{V}_{z_1} \cdot \mathcal{U}_{z_2}, \quad (63)$$

$$\mathcal{V}_{z_1} = \tilde{U}_{Z1Y} \cdot \prod_{j=1}^m \left(U_{3m+3}^{\mathcal{I}_{z,j}}(0) X_{3m+3,j} \text{CRZ}_{3m+1 \rightarrow 3m+3}^{\mathcal{I}_{z,j}^1, \mathcal{I}_{z,j}^0} \left(\frac{-2\tau}{\Delta z} \right) X_{3m+3,j} (U_{3m+3}^{\mathcal{I}_{z,j}}(0))^\dagger \right) \cdot \tilde{U}_{Z1Y}^\dagger,$$

$$\mathcal{U}_{z_2} = \tilde{U}_{X1Y} \cdot \text{CRZ}_{3m+1 \rightarrow 3m+3}^{\emptyset, \{3m+4\}} \left(\frac{-2\tau}{\Delta z} \right) \cdot \text{CRZ}_{3m+1 \rightarrow 3m+3}^{\emptyset, \{2m+1, \dots, 3m, 3m+4\}} \left(\frac{2\tau}{\Delta z} \right) \cdot \tilde{U}_{X1Y}^\dagger,$$

where $\mathcal{I}_{z,j} = \{2m+1, 2m+2, \dots, 2m+j\}$ and

$$\mathcal{I}_{z,j}^0 = \{3m+4\}, \quad \mathcal{I}_{z,j}^1 = \{2m+1, 2m+2, \dots, 2m+j\}.$$

Here $\tilde{U}_{Z1Y} = \mathbf{1}^{\otimes 3} \otimes U_Y \otimes \mathbf{1}^{\otimes 3m}$ and $\tilde{U}_{X1Y} = H \otimes \mathbf{1} \otimes U_Y \otimes \mathbf{1}^{\otimes 3m}$.

In summary, the approximation of the time evolution $\exp(-iH\tau)$ with H defined in (29) is given by

$$V(\tau) = \mathcal{U}_1 \mathcal{V}_2 \left(\mathcal{V}_x \mathcal{V}_y \mathcal{V}_z \otimes \mathbf{1}^{\otimes (n_s+n_p)} \right) = \mathcal{U}_1 \mathcal{V}_2 \prod_{\alpha=x,y,z} (\mathcal{V}_{\alpha 1} \mathcal{U}_{\alpha 2}) \otimes \mathbf{1}^{\otimes (n_s+n_p)}, \quad (64)$$

where \mathcal{U}_1 is defined in (44)-(45), \mathcal{V}_2 is defined in (51), and \mathcal{V}_x , \mathcal{V}_y and \mathcal{V}_z are defined in (61), (62) and (63), respectively.

5 Complexity analysis

In this section, we analyze the complexity of the previously constructed quantum circuits. We begin by demonstrating the approximation of the circuit implementation for $\exp(i\mathcal{H}\tau)$ with a time step τ , where

$$\mathcal{H} = \gamma \sum_{\alpha=1}^d \sum_{j=1}^n \eta_{\alpha} (e^{i\lambda_{\alpha}(s_j^-)_{\alpha}} + e^{-i\lambda_{\alpha}(s_j^+)_{\alpha}}) \quad (65)$$

as proved in [34]. Here η_{α} and γ are real scalar parameters, while $\lambda_{\alpha} \in \mathbb{R}$ is the phase parameter and

$$(s_j^{\mu})_{\alpha} = \mathbf{1}^{\otimes (\alpha-1)n} \otimes s_j^{\mu} \otimes \mathbf{1}^{\otimes (d-\alpha)n},$$

for $\mu \in \{+, -\}$.

Lemma 5.1. *The time evolution operator $\exp(-i\mathcal{H}\tau)$, with \mathcal{H} defined in (65), can be approximated by the unitary*

$$\bigotimes_{\alpha=1}^d V(\gamma\eta_{\alpha}\tau, \lambda_{\alpha}) = \prod_{\alpha=1}^d \mathbf{1}^{\otimes (\alpha-1)n} \otimes \left(\prod_{j=1}^n \mathbf{1}^{\otimes (n-j)} \otimes U_n^{\mathcal{I}_j}(\lambda) CRZ_j^{\mathcal{I}_j^1, \emptyset}(2\gamma\tau) (U_n^{\mathcal{I}_j}(-\lambda))^{\dagger} \right) \otimes \mathbf{1}^{\otimes (d-\alpha)n},$$

where $\mathcal{I}_j = \mathcal{I}_j^1 = \{1, 2, \dots, j-1\}$, $CRZ_j^{\mathcal{I}_j^1, \emptyset}(2\gamma\tau) = \exp(-i\gamma\tau Z \otimes \sigma_{11}^{\otimes (j-1)})$ is a multi-controlled $RZ(2\gamma\tau)$ gate acting on the j -th qubit when the $1, \dots, (j-1)$ -th qubits become 1. The approximation error is upper bounded in the sense of the operator norm as

$$\| \exp(-i\mathcal{H}\tau) - \bigotimes_{\alpha=1}^d V(\gamma\eta_{\alpha}\tau, \lambda_{\alpha}) \| \leq \frac{\gamma^2 \tau^2 (n-1)}{2} \sum_{\alpha=1}^d \eta_{\alpha}^2.$$

Lemma 5.2. *Consider the Schrödingerized equation $\frac{d}{dt}|\tilde{\mathbf{v}}_h\rangle = -iH|\tilde{\mathbf{v}}_h\rangle$ with the Hamiltonian H given in (29). The time evolution operator $\exp(-iH\tau)$ with the time step τ can be approximated by the unitary $V(\tau)$ in (64). The approximation error in the sense of the operator norm is upper bounded as*

$$\| \exp(-iH\tau) - V(\tau) \| \lesssim \frac{d\tau^2(m-1)}{\Delta x^2} + \frac{\tau^2 F_{\max}}{\Delta p \Delta x} + \frac{\tau^2 F_{\max}}{\Delta p \Delta s} + \frac{\tau^2}{\Delta s \Delta x} + \frac{(d+1)|\mathcal{I}||\mathcal{I}_s|F_{\max}^2\tau^2}{\Delta p}, \quad (66)$$

where $d=3$ is the dimension, $|\mathcal{I}| = \max_{\alpha=x,y,z,\rho,l \in \mathcal{I}_s} |\mathcal{I}_{\alpha}^l|$, $F_{\max} = \|\mathbf{F}\|_{\max}$.

Proof. Using Trotter's splitting and the triangle inequality, it yields

$$\begin{aligned} & \|\exp(-iH\tau) - V(\tau)\| \\ & \lesssim \tau^2 (\| [H_{D_s} + H_F, H_{\text{curl}}] \| + \| [H_{D_s}, H_F] \|) + \|\mathcal{U}_2 - \mathcal{V}_2\| + \|\mathcal{U}_3 - (\mathcal{V}_x \mathcal{V}_y \mathcal{V}_z) \otimes \mathbf{1}^{\otimes(n_s+n_p)}\|. \end{aligned} \quad (67)$$

In the following, we consider the approximation of the right-hand sides of (67) term by term.

Under the assumption that $\Delta x = \Delta y = \Delta z$, one has

$$\| [H_{D_s} + H_F, H_{\text{curl}}] \| \lesssim \| H_{D_s} + H_F \| \| H_{\text{curl}} \| \lesssim \frac{F_{\max}}{\Delta p \Delta x} + \frac{1}{\Delta s \Delta x}, \quad (68)$$

$$\| [H_{D_s}, H_F] \| \lesssim \| H_{D_s} \| \| H_F \| \lesssim \frac{F_{\max}}{\Delta s \Delta p}. \quad (69)$$

The error for $\|\mathcal{U}_2 - \mathcal{V}_2\|$ is bounded by

$$\begin{aligned} \|\mathcal{U}_2 - \mathcal{V}_2\| & \lesssim \sum_{\substack{\alpha=x,y,z,\rho \\ l \in \mathcal{I}_s, j \in \mathcal{I}_\alpha}} (\| [H_{X_p, l_j}^\alpha, H_{Y_p, l_j}^\alpha] \| + \| [H_{X_p, l_j}^\alpha, H_{Y_p, l_j}^\alpha] \| + \| [H_{X_p, l}^\alpha, H_{Y_p, l_j}^\alpha] \| + \| [H_{X_p, l}^\alpha, H_{Y_p, l}^\alpha] \|) \\ & \lesssim (d+1) |\mathcal{I}| |\mathcal{I}_s| \frac{F_{\max}^2}{\Delta p}, \end{aligned} \quad (70)$$

where $|\mathcal{I}| = \max_{\alpha=x,y,z,\rho} \max_{l \in \mathcal{I}_s} |\mathcal{I}_\alpha^l|$. This leads from Lemma 5.1 to the estimation of the last term in Equation (67) as follows

$$\begin{aligned} \|\mathcal{U}_3 - (\mathcal{V}_x \mathcal{V}_y \mathcal{V}_z) \otimes \mathbf{1}^{\otimes(n_s+n_p)}\| & \leq \|\mathcal{U}_3 - (\mathcal{U}_x \mathcal{U}_y \mathcal{U}_z) \otimes \mathbf{1}^{\otimes(n_s+n_p)}\| + \|\mathcal{U}_x - \mathcal{V}_x\| + \|\mathcal{U}_y - \mathcal{V}_y\| + \|\mathcal{U}_z - \mathcal{V}_z\| \\ & \lesssim \tau^2 (\| [H_x + H_y, H_z] \| + \| [H_x, H_y] \|) + \sum_{\alpha=x,y,z} \|\mathcal{U}_{\alpha_1} - \mathcal{V}_{\alpha_1}\| \\ & \lesssim \frac{\tau^2}{\Delta x^2} + \frac{d\tau^2(m-1)}{\Delta x^2}. \end{aligned} \quad (71)$$

Inserting (68)–(71) into (67), the proof is completed. \square

Lemma 5.3. *The approximation of $\exp(-iH\tau)$ denoted by $V(\tau)$, where H is the Hamiltonian defined in (29) and τ is the time step, can be implemented by $\mathcal{O}(dm + n_s + (d+1)|\mathcal{I}||\mathcal{I}_s|n_p)$ single-qubit gates and at most $\mathcal{O}(dm^2 + n_s^2 + (d+1)|\mathcal{I}||\mathcal{I}_s|n_p(n_s + md))$ CNOT gates, where $|\mathcal{I}| = \max_{\alpha=x,y,z,\rho} \max_{l \in \mathcal{I}_s} |\mathcal{I}_\alpha^l|$ and $n_p, n_s, m \geq d = 3$.*

Proof. Let $\mathcal{N}_S(\mathcal{U})$ be the number of single-qubit gates of the operator \mathcal{U} and $\mathcal{N}_{\text{CNOT}}(\mathcal{U})$ be the number of non-local gates of the operator \mathcal{U} . It is obvious that

$$\mathcal{N}_\beta(V(\tau)) = \mathcal{N}_\beta(\mathcal{U}_1) + \mathcal{N}_\beta(\mathcal{V}_2) + \sum_{\alpha=x,y,z} (\mathcal{N}_\beta(\mathcal{V}_{\alpha_1}) + \mathcal{N}_\beta(\mathcal{V}_{\alpha_2})),$$

where $\beta = \{S, \text{CNOT}\}$. According to Figure 2, the implementation of \mathcal{U}_1 just has a maximum of

$$\mathcal{N}_S(\mathcal{U}_1) = \mathcal{O}(n_s + 1) \quad (72)$$

single gates. The non-local gates included in the operator \mathcal{U}_1 are $\mathcal{O}(n_s^2)$ CR gates to implement the (inverse) quantum Fourier transform (QFT, IQFT), which corresponds to $\mathcal{O}(n_s^2)$ CNOT gates.

The number of single qubit gates and CNOT gates of \mathcal{V}_2 satisfies

$$\mathcal{N}_\beta(\mathcal{V}_2) = \sum_{l \in \mathcal{I}_s} \sum_{j \in \mathcal{I}_\alpha^l} \left(\mathcal{N}_\beta(\mathcal{U}_{X_p, l_j}^\alpha) + \mathcal{N}_\beta(\mathcal{U}_{Y_p, l_j}^\alpha) \right) + \left(\mathcal{N}_\beta(\mathcal{U}_{X_p, l}^\alpha) + \mathcal{N}_\beta(\mathcal{U}_{Y_p, l}^\alpha) \right), \quad (73)$$

where $\beta \in \{\text{S}, \text{CNOT}\}$. From Figures 3–5, one can find that the operator $\mathcal{U}_{X_p, l_j}^\alpha$ has n_p $\mathcal{U}_{X, l_j}^\alpha$ which is a multi-controlled RX gate, each consisting of $n_s + m(d + 1)$ control points, and $\mathcal{U}_{X_p, l}^\alpha$ has n_p multi-controlled RX gates, each of which has $n_s + 3$ control points. It is known from [47] that the multi-controlled RZ gate with $(j - 1)$ control qubits can be decomposed into single-qubit gates and at most $16j - 40$ CNOT gates. Therefore, the number of single-qubit and CNOT gates required to implement the operator $\mathcal{U}_{X_p, l_j}^\alpha$ and $\mathcal{U}_{X_p, l}^\alpha$ are

$$\mathcal{N}_\text{S}(\mathcal{U}_{X_p, l_j}^\alpha) = n_p, \quad \mathcal{N}_\text{CNOT}(\mathcal{U}_{X_p, l_j}^\alpha) = n_p(16(n_s + m(d + 1) + 1) - 24), \quad (74)$$

$$\mathcal{N}_\text{S}(\mathcal{U}_{X_p, l}^\alpha) = n_p, \quad \mathcal{N}_\text{CNOT}(\mathcal{U}_{X_p, l}^\alpha) = n_p(16(n_s + d + 1) - 24). \quad (75)$$

From Equation (56), one gets

$$\mathcal{N}_\text{S}(\mathcal{U}_{Y_p, l_j}^\alpha) = 1, \quad \mathcal{N}_\text{CNOT}(\mathcal{U}_{Y_p, l_j}^\alpha) = 16(n_s + m(d + 1)) - 24, \quad (76)$$

$$\mathcal{N}_\text{S}(\mathcal{U}_{Y_p, l}^\alpha) = 1, \quad \mathcal{N}_\text{CNOT}(\mathcal{U}_{Y_p, l}^\alpha) = 16(n_s + d + 1) - 24. \quad (77)$$

Inserting Equation (74)–(77) into Equation (73), the number of gates to implement \mathcal{V}_2 are

$$\mathcal{N}_\text{S}(\mathcal{V}_2) = \mathcal{O}((d + 1)|\mathcal{I}_s||\mathcal{I}|(n_p + 1)), \quad \mathcal{N}_\text{CNOT}(\mathcal{V}_2) = \mathcal{O}((d + 1)|\mathcal{I}_s||\mathcal{I}|(n_p n_s + d n_p m)), \quad (78)$$

where $|\mathcal{I}| = \max_{\alpha=x, y, z, \rho, l \in \mathcal{I}_s} |\mathcal{I}_\alpha^l|$, $d = 3$.

As shown in Figure 6, the operator W_j consists of a multi-controlled RZ₃ gate with $j + 1$ control points and a total of $2(j - 1)$ CNOT gates. Therefore, the number of CNOT gates and single-qubit gates required to implement the approximated \mathcal{V}_{x_1} is

$$\mathcal{N}_\text{S}(\mathcal{V}_{x_1}) = \mathcal{O}(m), \quad \mathcal{N}_\text{CNOT}(\mathcal{V}_{x_1}) = \mathcal{O}(m^2). \quad (79)$$

From Figure 7, it yields similarly

$$\mathcal{N}_\text{S}(\mathcal{U}_{x_2}) = \mathcal{O}(1), \quad \mathcal{N}_\text{CNOT}(\mathcal{U}_{x_2}) = \mathcal{O}(m + 1). \quad (80)$$

In summary, from (72)–(80), one has

$$\begin{aligned} \mathcal{N}_\text{S}(V(\tau)) &= \mathcal{O}(dm + n_s + (d + 1)|\mathcal{I}||\mathcal{I}_s|n_p), \\ \mathcal{N}_\text{CNOT}(V(\tau)) &= \mathcal{O}(dm^2 + n_s^2 + (d + 1)|\mathcal{I}||\mathcal{I}_s|n_p(n_s + md)), \end{aligned}$$

where $d = 3$. The proof is finished. \square

5.1 Main results

In this subsection, we present the main result of the complexity of the Schrödingerisation for Maxwell's equations. Before that, we give the error estimates of the spectral methods (see for example [37]).

Lemma 5.4. For $u \in H_p^m(I)$ which consists of functions with derivatives of order up to $m - 1$ being $2\pi L$ -periodic, there holds

$$\|u - \mathcal{I}_N u\|_{L^2(I)} \lesssim \Delta p^m |u|_{H^m(I)}, \quad (81)$$

where \mathcal{I}_N is the discrete Fourier interpolation by

$$\mathcal{I}_N u(p) = \sum_{k=-N/2}^{N/2} \tilde{u}_k e^{ik(p/L+\pi)}, \quad \tilde{u}_k = \frac{1}{N c_k} \sum_{j=0}^{N-1} u(p_j) e^{-ik(p_j/L+\pi)}, \quad k = -N/2, \dots, N/2, \quad (82)$$

where $c_k = 1$ for $|k| < N/2$, and $c_k = 2$ for $k = \pm N/2$.

Lemma 5.5. Assume L and S are large enough such that $e^{-S\pi+T} \approx e^{-L\pi+T/2} \approx 0$, and $g(p) \in C^r(\mathbb{R})$, $\beta(\xi) \in H^r(\mathbb{R})$ is the r -th order approximation to the δ function. Define $\mathbf{v}_h^D(T) = \mathcal{V} \mathbf{v}_h(0)$ and $\mathbf{u}_h^D|k\rangle = e^{p_k} \Delta s \sum_{l \in [N_s]} (I_n \otimes \langle l | \otimes I_{N_p}) M_k \mathbf{v}_h^D$, where $\mathcal{V} = (I_n \otimes I_{N_s} \otimes \Phi^p) V^{N_t}(\tau) (I_n \otimes I_{N_s} \otimes (\Phi^p)^\dagger)$. The relative error holds as follows

$$\frac{\|\mathbf{u}_h^D|k\rangle - \mathbf{u}_f|k\rangle\|}{\|\mathbf{u}_f(T)\|} \lesssim \frac{e^{p_k} \|\mathbf{u}_f(0)\|}{\|\mathbf{u}_f(T)\|} \|\mathcal{V} - \mathcal{U}\| + \Delta p^r + \Delta s^r, \quad (83)$$

where $\mathcal{U} = (I_n \otimes I_{N_s} \otimes \Phi^p) U (I_n \otimes I_{N_s} \otimes (\Phi^p)^\dagger)$, and $p_k \geq T/2$.

Proof. Since $e^{-\pi L+T/2} \approx 0$ and $g(p) \in C^r(\mathbb{R})$, the error bounded by the spectral method is obtained from Lemma 5.4 such that

$$\frac{\|\mathbf{M}_k \mathbf{w}_h - e^{-p_k} \mathbf{u}_f|k\rangle\|}{\|\mathbf{w}(t, p_k)\|} \leq \mathcal{O}(\Delta p^r), \quad (84)$$

where $\mathbf{M}_k = I_n \otimes |k\rangle\langle k|$ and we use $\mathbf{w}(t, p_k) = e^{-p_k} \mathbf{u}$ for $p_k \geq T/2$ from the recovery Theorem 3.2.

Since \mathbf{v} satisfies the transport equation in the s direction, and $\beta(\xi) \in H^r(\mathbb{R})$ is the r -th-order approximation to the δ function, one gets the error between the semi-discrete solution \mathbf{w}_h^D in Equation (28) and \mathbf{w}_h in Equation (25)-(26) from Lemma 5.4

$$\frac{\|\mathbf{M}_k(\mathbf{w}_h^D - \mathbf{w}_h)\|}{\|\mathbf{w}(t, p_k)\|} \leq \mathcal{O}(\Delta s^r), \quad (85)$$

under the assumption $e^{-\pi S+T} \approx 0$. Here we used the relation $\|\mathbf{M}_k \mathbf{w}_h\| = (1 + \mathcal{O}(\Delta p^r)) \|\mathbf{w}(t, p_k)\|$ from Equation (84). According to Equation (84)-(85), one has the relative error as follows

$$\begin{aligned} \frac{\|\mathbf{u}_h^D|k\rangle - \mathbf{u}_f|k\rangle\|}{\|\mathbf{u}_f(T)\|} &= \frac{\|e^{p_k} \Delta s \sum_{l \in [N_s]} (I_n \otimes \langle l | \otimes I_{N_p}) M_k \mathcal{V} \mathbf{v}_h(0) - \mathbf{u}_f|k\rangle\|}{\|\mathbf{u}_f(T)\|} \\ &\leq \frac{e^{p_k}}{\|\mathbf{u}_f(T)\|} \left\| \Delta s \sum_{l \in [N_s]} (I_n \otimes \langle l | \otimes I_{N_p}) M_k (\mathcal{V} - \mathcal{U}) \mathbf{v}_h(0) \right\| \\ &\quad + \frac{1}{\|\mathbf{w}(T, p_k)\|} \left\| \Delta s \sum_{l \in [N_s]} (I_n \otimes \langle l | \otimes I_{N_p}) M_k \mathcal{U} \mathbf{v}_h(0) - \mathbf{M}_k \mathbf{w}_h \right\| + \left\| \frac{e^{p_k}}{\|\mathbf{u}_f(T)\|} \mathbf{w}_h(t, p_k) - \mathbf{u}_f|k\rangle \right\| \\ &\lesssim \frac{e^{p_k} \|\mathbf{u}_f(0)\|}{\|\mathbf{u}_f(T)\|} \|\mathcal{V} - \mathcal{U}\| + \Delta p^r + \Delta s^r. \end{aligned}$$

Here we have used $\mathbf{w}(t, p_k) = e^{-p_k} \mathbf{u}_f(t)$ and $\|\Delta s \sum_{l \in [N_s]} (I_n \otimes \langle l | \otimes I_{N_p}) M_k \mathbf{v}_h(0)\| = \mathcal{O}(\|\mathbf{u}_f(0)\|)$. \square

Theorem 5.1. *Given Maxwell's equations with time dependent source term, then $\mathbf{u}_f(t)$, the solution of Equation (17) with a mesh size $\Delta x = \Delta y = \Delta z = 1/M$, $m = \log_2 M$, can be prepared with precision ε using the Schrödingerisation method depicted in Figure 1. Assume the assumptions in Lemma 5.5 and Assumption 4.1 hold, this preparation can be achieved using at most*

$$\tilde{\mathcal{O}} \left(\frac{T^2 e^{\frac{3}{2}} \|\mathbf{u}_f(0)\|^3}{\varepsilon \|\mathbf{u}_f(T)\|^3} (M^2 d^2 m (|\mathcal{I}||\mathcal{I}_s| + m) + \frac{(dF_{\max} |\mathcal{I}||\mathcal{I}_s|)^2}{\sqrt{\varepsilon}}) \right)$$

single-qubit gates and

$$\tilde{\mathcal{O}} \left(\frac{T^2 e^{\frac{3}{2}} \|\mathbf{u}_f(0)\|^3}{\varepsilon \|\mathbf{u}_f(T)\|^3} (M^2 d^2 m^2 (d|\mathcal{I}||\mathcal{I}_s| + m) + \frac{md(dF_{\max} |\mathcal{I}||\mathcal{I}_s|)^2}{\sqrt{\varepsilon}}) \right)$$

CNOT gates.

Proof. We divide the time into equal intervals, with the time step defined as $\tau = T/N_t$. For the simulation accuracy to be within ε , according to Lemma 5.5, one needs to choose the number of simulation steps N_t and mesh size Δp , Δs to satisfy the following conditions

$$\|\mathcal{U} - \mathcal{V}\| = \|U^{N_t}(\tau) - V^{N_t}(\tau)\| \leq N_t \|U(\tau) - V(\tau)\| \leq \frac{e^{-p_k} \|\mathbf{u}_f(T)\|}{\|\mathbf{u}_f(0)\|} \varepsilon, \quad (86)$$

$$\Delta p \sim \Delta s \sim \sqrt[3]{\varepsilon}. \quad (87)$$

Combined with Lemma 5.2, N_t should be large enough such that

$$N_t \geq \frac{T^2 e^{p_k} \|\mathbf{u}_f(0)\|}{\varepsilon \|\mathbf{u}_f(T)\|} \left(\frac{d(m-1)}{\Delta x^2} + \frac{F_{\max}}{\sqrt[3]{\varepsilon} \Delta x} + \frac{F_{\max}}{\sqrt[3]{\varepsilon}^2} + \frac{1}{\sqrt[3]{\varepsilon} \Delta x} + \frac{F_{\max}^2 |\mathcal{I}||\mathcal{I}_s| d}{\sqrt[3]{\varepsilon}} \right).$$

From Equation (87), one has

$$N_p = \frac{2\pi L}{\Delta p} = \mathcal{O}\left(\frac{\ln(\frac{1}{\varepsilon})}{\sqrt[3]{\varepsilon}}\right), \quad n_p = \log_2 N_p = \mathcal{O}\left(\log\left(\frac{\ln(\frac{1}{\varepsilon})}{\sqrt[3]{\varepsilon}}\right)\right), \quad (88)$$

$$N_s = \frac{2\pi S}{\Delta s} = \mathcal{O}\left(\frac{\ln(\frac{1}{\varepsilon})}{\sqrt[3]{\varepsilon}}\right), \quad n_s = \log_2 N_s = \mathcal{O}\left(\log\left(\frac{\ln(\frac{1}{\varepsilon})}{\sqrt[3]{\varepsilon}}\right)\right), \quad (89)$$

where we have used the assumption $e^{-\pi S+T} \approx e^{-\pi L+\frac{T}{2}} \approx 0 \leq \varepsilon$. Therefore, the numbers of single-qubit gates and CNOT gates to implement $V^{N_t}(\tau)$ are, respectively,

$$\begin{aligned} \mathcal{N}_S(V^{N_t}(\tau)) &= \mathcal{O}(N_t \mathcal{N}_S(V(\tau))) \\ &\leq \mathcal{O}\left(\frac{T^2 e^{p_k} \|\mathbf{u}_f(0)\|}{\varepsilon \|\mathbf{u}_f(T)\|} (d|\mathcal{I}||\mathcal{I}_s| \log\left(\frac{\ln(\frac{1}{\varepsilon})}{\sqrt[3]{\varepsilon}}\right) + md) \cdot \left(M^2 dm + \frac{F_{\max}(M + dF_{\max} |\mathcal{I}_s| |\mathcal{I}|)}{\sqrt[3]{\varepsilon}}\right)\right) \\ &= \tilde{\mathcal{O}}\left(\frac{T^2 e^{p_k} \|\mathbf{u}_f(0)\|}{\varepsilon \|\mathbf{u}_f(T)\|} \left(M^2 d^2 m (|\mathcal{I}||\mathcal{I}_s| + m) + \frac{(dF_{\max} |\mathcal{I}||\mathcal{I}_s|)^2}{\sqrt[3]{\varepsilon}}\right)\right), \\ \mathcal{N}_{\text{CNOT}}(V^{N_t}(\tau)) &= \mathcal{O}(N_t \mathcal{N}_{\text{CNOT}}(V(\tau))) \\ &\leq \tilde{\mathcal{O}}\left(\frac{T^2 e^{p_k} \|\mathbf{u}_f(0)\|}{\varepsilon \|\mathbf{u}_f(T)\|} \left(M^2 d^2 m^2 (d|\mathcal{I}||\mathcal{I}_s| + m) + \frac{md(dF_{\max} |\mathcal{I}||\mathcal{I}_s|)^2}{\sqrt[3]{\varepsilon}}\right)\right). \end{aligned}$$

Next, we consider the probability of getting the desired state

$$M_k |v_h^D\rangle \approx \frac{e^{-p_k} \mathbf{u}_f(T) |k\rangle \otimes \delta_h}{\|v_h^D(T)\|} \approx \frac{e^{-p_k} \|\mathbf{u}_f(T)\|}{\|\mathbf{u}_f(0)\|} |\mathbf{u}_f(T)\rangle |k\rangle |\delta_h(T)\rangle.$$

The first approximation is from Lemma 5.5 and Equation (86). Therefore, $\mathcal{O}\left(\frac{e^{2p_k} \|\mathbf{u}_f(0)\|^2}{\|\mathbf{u}_f(T)\|^2}\right)$ measurements are needed. The proof is finished by choosing $p_k = T/2$. \square

Remark 5.1. From (15), by applying Duhamel's principle, one gets

$$\mathbf{u}_T = \mathbf{u}(T) = e^{AT} \mathbf{u}_0 + \int_0^T e^{A(T-s)} \mathbf{f}(s) ds.$$

Since A is skew Hermitian, one has

$$\|\mathbf{u}_T\|^2 = \|\mathbf{u}_0\|^2 + 2\mathbf{u}_0^\top \tilde{\mathbf{f}} + \|\tilde{\mathbf{f}}\|^2,$$

where $\tilde{\mathbf{f}} = \int_0^T e^{-As} \mathbf{f}(s) ds$ and $\|\tilde{\mathbf{f}}\| \leq \|\int_0^T \mathbf{f}(s) ds\|$. Consequently, it follows that $\|\mathbf{u}_T\|/\|\mathbf{u}_0\| = \mathcal{O}(1)$ for any fixed $T = \mathcal{O}(1)$, provided that the source terms satisfy $\mathbf{J}, \rho \in L^\infty(0, T; L^2(\Omega))$. Considering $\mathbf{u}_f(T) = \mathbf{u}(T) + \mathbf{r}$, it follows

$$\frac{\|\mathbf{u}_f(0)\|^2}{\|\mathbf{u}_f(T)\|^2} = \frac{\Delta x^d \|\mathbf{u}_0\|^2 + 8c_0^2}{\Delta x^d \|\mathbf{u}_T\|^2 + 8c_0^2} \approx \frac{\|\mathbf{E}_0\|_{L^2(\Omega)}^2 + \|\mathbf{B}_0\|_{L^2(\Omega)}^2 + 8c_0^2}{\mathcal{O}(\|\mathbf{E}_0\|_{L^2(\Omega)}^2 + \|\mathbf{B}_0\|_{L^2(\Omega)}^2) + 8c_0^2}$$

Here we used the numerical integration $\Delta x^d \|\mathbf{u}_0\|^2 \approx \|\mathbf{E}(0)\|_{L^2(\Omega)}^2 + \|\mathbf{B}(0)\|_{L^2(\Omega)}^2$. Noting that $c_0 = \max\{\max_{t \in (0, T)} \|\mathbf{f}\|_{l^\infty}, 1\} \leq \max\{\max_{t \in (0, T)} \mathbf{J}, \max_{t \in (0, T)} \rho, 1\} = \mathcal{O}(1)$, one has $\|\mathbf{u}_f(0)\|/\|\mathbf{u}_f(T)\| = \mathcal{O}(1)$. Therefore, introducing an auxiliary variable \mathbf{r} to obtain a homogeneous equation (16) does not impose a significant additional computational burden.

5.1.1 Comparison with the classical algorithm (FDTD)

To achieve an approximate solution with accuracy ε using a second-order spatial discretization, we choose $M = 1/\sqrt{\varepsilon}$ and $m \sim \log(1/\sqrt{\varepsilon})$. According to Theorem 5.1, the computation cost for single-qubit and CNOT gates is at most

$$\tilde{\mathcal{O}} \left(\frac{T^2 e^{3T/2} \|\mathbf{u}_f(0)\|^3 d^3}{\|\mathbf{u}_f(T)\|^3} \left(\frac{1}{\varepsilon^2} \left(\log \left(\frac{1}{\sqrt{\varepsilon}} \right) \right) + \frac{F_{\max}^2}{\varepsilon^{1/r+1}} \right) \right) = \tilde{\mathcal{O}} \left(d^3 \varepsilon^{-2} \log \left(\frac{1}{\sqrt{\varepsilon}} \right) \right), \quad r \geq 2.$$

In comparison, classical algorithms, such as the explicit Finite-Difference Time-Domain (FDTD) method, incur a computational cost of $\mathcal{O}(\varepsilon^{-1-\frac{d}{2}})$. Our quantum algorithms, derived via Schrödingerization, demonstrate a modest advantage in computational complexity when $d = 3$.

To further enhance the advantages of quantum computing, we can employ a higher-order Trotter-Suzuki formula [12] for $\mathcal{H} = \sum_{l=1}^k \gamma_l \mathcal{H}_l$ such that

$$\left(\prod_{j=1}^k \exp(-i \frac{\gamma_j \mathcal{H}_j T}{2N_t}) \prod_{j=k}^1 \exp(-i \frac{\gamma_j \mathcal{H}_j T}{2N_t}) \right)^{N_t} = \exp(-i \mathcal{H} T) + \mathcal{O} \left(\frac{(khT)^3}{N_t^2} \right), \quad (90)$$

where $h = \max_j \|\mathcal{H}_j\|$. For the Hamiltonian H defined in (39)–(41), with H_F and H_{curl} reformulated in Equation 50 and Equation (58), respectively, achieving an approximation with precision ε requires the time step N_t to satisfy

$$N_t = \mathcal{O} \left(\frac{1}{\sqrt{\varepsilon}} \left(\frac{md + n_s + d|\mathcal{I}||\mathcal{I}_s|n_p}{\Delta x} \right)^{\frac{3}{2}} \right). \quad (91)$$

Since the number of gates required to implement the circuit is doubled, the computational cost for single-qubit and CNOT gates remains at most

$$\tilde{\mathcal{O}} \left(\varepsilon^{-\frac{5}{4}} \log \left(\frac{1}{\sqrt{\varepsilon}} \right) \right), \quad (92)$$

when $d = \mathcal{O}(1)$. This represents a significant acceleration compared to classical algorithms.

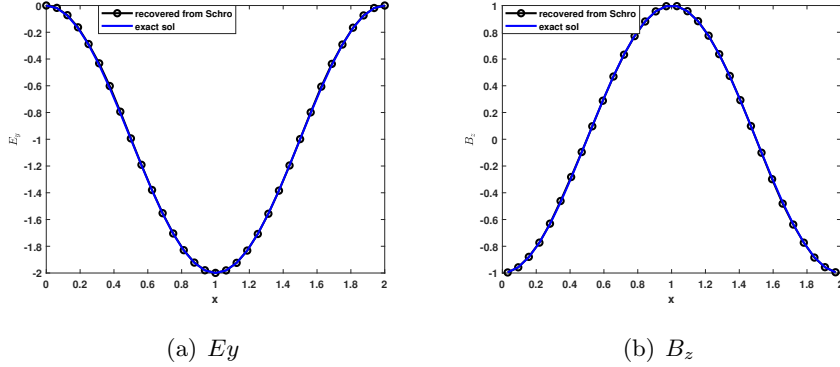


Figure 8: Simulation of electromagnetic fields by Schrödingerisation at $T = 1/2$ with the truncated domain restricted to $p \in (-4\pi, 4\pi)$, $s \in (-5, 5)$, and mesh size $\Delta x = \frac{1}{2^4}$, $\Delta s = \frac{10}{2^7}$, $\Delta p = \frac{8\pi}{2^7}$.

6 Numerical tests

For the numerical experiments, we utilize a classical computer to simulate the Hamiltonian system, verifying the practicality of the algorithms above, particularly focusing on the high-order accuracy of the scheme and recovery from Schrödingerisation. To simplify the presentation, we restrict ourselves to a reduced version of the Maxwell equations with one spatial variable, x , namely

$$\begin{aligned} \partial_t E_y + \partial_x B_z &= -J_y, & \partial_t B_z + \partial_x E_y &= 0, & \text{in } [0, 2], \\ E_y(0) &= 0, & E_y(2) &= 0. \end{aligned}$$

In order to test the accuracy of the algorithm, we set the exact solution as

$$E_y = \sin(\pi(x+t)) - \sin(\pi t), \quad B_z = -\sin(\pi(x+t)). \quad (93)$$

In this numerical test, we truncate the p region to $(-4\pi, 4\pi)$ and the s region to $(-5, 5)$. The simulation stops at $T = 1/2$. We examine the convergence rates of Schrödingerization concerning p and s variables with fixed $\Delta x = 1/2^4$. The result of the above simulation is shown in Figure 8, which shows that the numerical solutions from Schrödingerisation are in agreement with the exact solutions.

As shown in Table 1, a second-order convergence is achieved owing to the smoothness of $g(p) \in C^2(\mathbb{R})$, $\beta(\xi) \in H^2(\mathbb{R})$, and the utilization of second-order temporal discretization schemes.

$(\Delta p, \Delta s, \Delta t)$	$(\frac{8\pi}{2^5}, \frac{10}{2^5}, \frac{1}{2^6})$	order	$(\frac{8\pi}{2^6}, \frac{10}{2^6}, \frac{1}{2^7})$	order	$(\frac{8\pi}{2^7}, \frac{10}{2^7}, \frac{1}{2^8})$	order
$\ E_{\text{schr}} - E_h\ _{l^\infty}$	4.5819e-01	-	1.0865e-01	2.07	1.5440e-02	2.81
$\ B_{\text{schr}} - B_h\ _{l^\infty}$	4.2349e-01	-	1.0732e-01	1.98	9.7667e-03	3.45

Table 1: The convergence rates of $\|E_{\text{schr}} - E_h\|_{l^\infty}$ and $\|B_{\text{schr}} - B_h\|_{l^\infty}$, respectively, where E_h and B_h are the solutions to Equation (8)–(9), E_{schr} and B_{schr} are the recovery from the Schrödingerisation according to Equation (32) with $k := \min_j \{j : p_j > 0.5\}$.

7 Conclusions

The Schrödingerisation method, in conjunction with the autonomization approach in [10], transforms time-varying linear partial and ordinary differential equations with non-unitary dynamics into time-independent Schrödinger-type equations. This transformation is achieved through a warped phase transformation that maps the equations into two higher dimensions. In this paper, we present a detailed implementation and accordingly the detailed computational complexity analysis of quantum circuits for the Schrödingerisation of Maxwell's equations under Perfect Electric Conductor (PEC) boundary conditions and time-varying source terms. Through the application of smooth extension in the initial data of the extended space, and high-order approximations to the delta function, the rise in dimensionality due to the transformation does not increase the computational load of quantum computations, only $\mathcal{O}(\log \log(1/\varepsilon))$ with ε the desired precision. In addition, transforming source-driven ODE systems into homogeneous systems by introducing auxiliary variables with the stretch transformation [21] does not diminish the success probability of obtaining the target states.

Acknowledgements

SJ, NL and LZ are supported by NSFC grant No. 12341104, the Shanghai Jiao Tong University 2030 Initiative and the Fundamental Research Funds for the Central Universities. SJ was also partially supported by the Shanghai Municipal Science and Technology Major Project (2021SHZDZX0102). NL also acknowledges funding from the Science and Technology Program of Shanghai, China (21JC1402900). LZ is also partially supported by the Shanghai Municipal Science and Technology Project 22JC1401600. CM was partially supported by China Postdoctoral Science Foundation (No. 2023M732248) and Postdoctoral Innovative Talents Support Program (No. BX20230219).

References

- [1] D. An, A. M. Childs, and L. Lin. Quantum algorithm for linear non-unitary dynamics with near-optimal dependence on all parameters. *arXiv preprint arXiv:2312.03916*, 2023.
- [2] D. An, D. Fang, and L. Lin. Time-dependent unbounded Hamiltonian simulation with vector norm scaling. *Quantum*, 5:459, 2021.
- [3] D. An, D. Fang, and L. Lin. Time-dependent Hamiltonian simulation of highly oscillatory dynamics and superconvergence for schrödinger equation. *Quantum*, 6:690, 2022.
- [4] D. An, J. Liu, and L. Lin. Linear combination of Hamiltonian simulation for non-unitary dynamics with optimal state preparation cost. *Phys. Rev. Lett.*, 131(150603), 2023.
- [5] F. Arute, K. Arya, R. Babbush, D. Bacon, J. C Bardin, R. Barends, and et al. Quantum supremacy using a programmable superconducting processor. *Nature*, 574(7779):505–510, 2019.

- [6] F. Assous, P. Ciarlet, and S. Labrunie. *Mathematical foundations of computational electromagnetism*. Springer International Publishing AG, 2018.
- [7] D. W. Berry, A. M Childs, R. Cleve, R. Kothari, and R. D Somma. Simulating Hamiltonian Dynamics with a truncated Taylor series. *Phys. Rev. Lett.*, 114(9), 2015.
- [8] D. W. Berry, A. M Childs, R. Cleve, R. Kothari, and R. D Somma. Exponential improvement in precision for simulating sparse Hamiltonians. *Forum of Mathematics, Sigma*, 5, 2017.
- [9] N. Bui, A. Reineix, and C. Guiffaut. Alternative quantum circuit implementation for 2d electromagnetic wave simulation with quasi-PEC modeling. *IEEE MTT-S International Conference on Electromagnetic and Multiphysics Modeling and Optimization*, 2022.
- [10] Y. Cao, S. Jin, and N. Liu. Quantum simulation for time-dependent Hamiltonians – with applications to non-autonomous ordinary and partial differential equations. *arXiv:2312.02817v1*, 2023.
- [11] S. Chakraborty, A. Gilyén, and S. Jeffery. The power of block-encoded matrix powers: Improved regression techniques via faster Hamiltonian simulation. In *Proceedings of the 46th International Colloquium on Automata, Languages, and Programming (ICALP 2019)*, 2019.
- [12] A. M. Childs, D. Maslov, Y. Nam, N. J. Ross, and Y. Su. Toward the first quantum simulation with quantum speedup. *Proceedings of the National Academy of Sciences*, 115(38):9456–9461, 2018.
- [13] P. C. Costa, S. Jordan, and A. Ostrander. Quantum algorithm for simulating the wave equation. *Phys. Rev. A*, 99(1):012323, 2019.
- [14] D. DiVincenzo. Quantum computation. *Science*, 270(5234):255–261, 1995.
- [15] D. Fang, L. Lin, and Y. Tong. Time-marching based quantum solvers for time-dependent linear differential equations. *Quantum*, 7:955, 2023.
- [16] J. Hu, S. Jin, N. Liu, and L. Zhang. Quantum circuits for partial differential equations via schrödingerisation. *ArXiv:2403.10032*, 2024.
- [17] J. Y. Huang, R. Y. Su, W. Han Lim, and et al. High-fidelity spin qubit operation and algorithmic initialization above 1 k. *Nature*, 627:8005, 2024.
- [18] S. Jin, X. Li, N. Liu, and Y. Yu. Quantum simulation for partial differential equations with physical boundary or interface conditions. *J. Comput. Phys.*, 498:112707, 2024.
- [19] S. Jin, X. Li, N. Liu, and Y. Yu. Quantum simulation for quantum dynamics with artificial boundary conditions. *SIAM J. Sci. Comput.*, 46(4):B403–B421, 2024.
- [20] S. Jin and N. Liu. Quantum simulation of discrete linear dynamical systems and simple iterative methods in linear algebra. *Proceedings of the Royal Society A*, 480(2291):20230370, 2024.

- [21] S. Jin, N. Liu, and C. Ma. On Schrödingerisation based quantum algorithms for linear dynamical systems with inhomogeneous terms. *arXiv preprint arXiv:2402.14696*, 2024.
- [22] S. Jin, N. Liu, and C. Ma. Quantum simulation of Maxwell’s equations via schrödingerisation. *ESAIM Math. Model. Numer. Anal.*, 58(5):1853-1879, 2024.
- [23] S. Jin, N. Liu, and C. Ma. Schrödingerisation based computationally stable algorithms for ill-posed problems in partial differential equations. *arXiv preprint arXiv:2403.19123*, 2024.
- [24] S. Jin, N. Liu, and Y. Yu. Quantum simulation of partial differential equations via schrodingerisation: technical details. *arXiv preprint arXiv:2212.14703*, 2022.
- [25] S. Jin, N. Liu, and Y. Yu. Quantum simulation of partial differential equations: Applications and detailed analysis. *Phys. Rev. A* , 108(3):032603, 2023.
- [26] S. Jin, N. Liu, and Y. Yu. Quantum circuits for the heat equation with physical boundary conditions via schrödingerisation. *arXiv:2407.15895*, 2024.
- [27] S. Jin, N. Liu, and Y. Yu. Quantum simulation of the Fokker-Planck equation via Schrödingerisation. *arXiv preprint arXiv:2404.13585*, 2024.
- [28] M. Kieferová, A. Scherer, and D. W. Berry. Simulating the dynamics of time-dependent Hamiltonians with a truncated Dyson series. *Phys. Rev. A*, 99:042314, 13 pp., 2019.
- [29] B. Lo, V. Minden, and P. Colella. A real-space green’s function method for the numerical solution of Maxwell’s equations. *COMM. APP. MATH. AND COMP. SCI.*, 11:143–170, 2016.
- [30] G. H. Low and I. L. Chuang. Optimal hamiltonian simulation by quantum signal processing. *Phys. Rev. Lett.*, 118(1):010501, 2017.
- [31] G. H. Low and I. L. Chuang. Hamiltonian simulation by qubitization. *Quantum*, 3:163, 2019.
- [32] M. Nagy and S. G. Akl. Quantum computing: Beyond the limits of conventional computation. *The International Journal of Parallel, Emergent and Distributed Systems*, 22:123–135, 2002.
- [33] S. J. Plimpton, S. G. Moore, A. Borner, A. K. Stagg, T. P. Koehler, J. R. Torczynski, and M. A. Gallis. *Physics of Fluids*, 31(8), 2019.
- [34] Y. Sato, R. Kondo, I. Hamamura, T. Onodera, and N. Yamamoto. Hamiltonian simulation for time-evolving partial differential equation by scalable quantum circuits. *arXiv:2402.18398*, 2024.
- [35] Y. Sato, H. Tezuka, R. Kondo, and N. Yamamoto. Quantum algorithm for partial differential equations of non-conservative systems with spatially varying parameters. *arXiv:2407.05019*, 2024.
- [36] M. Schade, C. Bösch, V. Hapla, and A. Fichtner. A quantum computing concept for 1-d elastic wave simulation with exponential speedup. *Geophysical Journal International*, 238(1):321–333, 2024.

- [37] J. Shen, T. Tang, and L. Wang. *Spectral methods*. Springer-Verlag Berlin Heidelberg, 2011.
- [38] P.W. Shor. Algorithms for quantum computation: discrete logarithms and factoring. *In: Proceedings of 35th Annual Symposium on Foundations of Computer Science*, pages 124–134, 1994.
- [39] A. Steane. Quantum computing. *Rep. Progr. Phys.*, 61(2):117–173, 1998.
- [40] A. Suau, G. Staffelbach, and H. Calandra. Practical quantum computing: Solving the wave equation using a quantum approach. *ACM Trans. Quantum Comput.*, 2(1):1–35, 2021.
- [41] A. Taflove, S. C. Hagness, and M. Piket-May. Computational electromagnetics: the finite-difference time-domain method. *The Electrical Engineering Handbook*, 3:629–670, 2005.
- [42] A.-K. Tornberg and B. Engquist. Numerical approximations of singular source terms in differential equations. *J. Comput. Phys.*, 200:462–488, 2004.
- [43] G. Vahala, L. Vahala, M. Soe, and A. K. Ram. The effect of the pauli spin matrices on the quantum lattice algorithm for Maxwell equations in inhomogeneous media. *10.48550/arXiv.2010.12264*, 2020.
- [44] G. Vahala, L. Vahala, M. Soe, and A. K. Ram. Unitary quantum lattice simulations for Maxwell equations in vacuum and in dielectric media. *J. Plasma. Phys.*, 86(5):905860518, 2020.
- [45] G. Vahala, L. Vahala, M. Soe, and A. K. Ram. One- and two-dimensional quantum lattice algorithms for Maxwell equations in inhomogeneous scalar dielectric media i: theory. *Radiat. Eff. Defect. S.*, 176(1):49–63, 2021.
- [46] G. Vahala, L. Vahala, M. Soe, and A. K. Ram. One- and two-dimensional quantum lattice algorithms for Maxwell equations in inhomogeneous scalar dielectric media ii: simulations. *Radiat. Eff. Defect. S.*, 176(2):64–72, 2021.
- [47] R. Vale, T. M. D. Azevedo, I. C. S. Araújo, I. F. Araujo, and A. J. da Silva. Circuit decomposition of multicontrolled special unitary single-qubit gates. *IEEE Transactions on Computer-Aided Design of Integrated Circuits and Systems*, 43:802–811, 2024.
- [48] B. Wang, G. Miller, and P. Colella. A particle-in-cell method with adaptive phase-space remapping for kinetic plasmas. *SIAM J. Sci. Comput.*, 33:3509–3537, 2011.
- [49] K. Yee. Numerical solution of initial boundary value problems involving Maxwell’s equations in isotropic media. *IEEE Transactions on antennas and propagation*, 14:302–307, 1966.
- [50] H. Zhong, H. Wang, Y. Deng, and et al. Quantum computational advantage using photons. *Science*, 370(6523):1460–1463, 2020.
- [51] S. Zuo, D. G. Doñoro, Y. Zhang, Y. Bai, and X. Zhao. Simulation of challenging electromagnetic problems using a massively parallel finite element method solver. *IEEE Access*, 7:20346–20362, 2019.